



Genesis of HDT catalysts prepared with the use of $\text{Co}_2\text{Mo}_{10}\text{HPA}$ and cobalt citrate: Study of their gas and liquid phase sulfidation



P.A. Nikulshin ^{a,*}, A.V. Mozhaev ^a, K.I. Maslakov ^b, A.A. Pimerzin ^a, V.M. Kogan ^c

^a Samara State Technical University, 244 Molodogvardiyskaya st., Samara 443100, Russia

^b Chemistry Department, M.V. Lomonosov Moscow State University, Lenins Hills 1, bld. 3, Moscow 119991, Russia

^c N.D. Zelinsky Institute of Organic Chemistry, RAS, 47 Leninsky prospekt, Moscow 119991, Russia

ARTICLE INFO

Article history:

Received 13 February 2014

Received in revised form 3 April 2014

Accepted 7 April 2014

Available online 18 April 2014

Keywords:

Hydrotreating

Heteropolycompounds

CoMoS

Genesis

Deactivation

ABSTRACT

Genesis of alumina supported hydrotreating (HDT) catalysts prepared with the use of decamolyb-dodicobaltate heteropolyanion ($\text{Co}_2\text{Mo}_{10}\text{HPA}$) and cobalt citrate during their sulfidation processes and deactivation in diesel HDT has been investigated. The sulfidation stage was studied for two procedures: gas phase sulfidation by $\text{H}_2\text{S}/\text{H}_2$ and liquid phase treatment by a mixture of dimethyldisulfide in diesel at various temperatures and durations. The catalysts have been studied by N_2 adsorption, thermogravimetric analysis, X-ray photoelectron spectroscopy and high-resolution transmission electron microscopy methods. The catalysts were tested in HDT of mixture of 70 wt.% straight run gas oil with 16 wt.% light cycle oil and 14 wt.% light coker gas oil. Mechanisms of the active phase formation in the course of gas and liquid phase sulfidation processes have been established. It was found that gas phase sulfidation led to formation of the CoMoS active phase with higher cobalt content comparing to liquid sulfidation of the catalyst and initial activity of the gas phase treated catalysts in diesel HDT was also higher than catalysts subjected to liquid sulfidation. Catalytic examination after accelerated deactivation conditions showed that the liquid phase sulfided sample was more resistant to the deactivation. Probably it is due to stabilization of active phase particles by coke formed intensively during liquid phase sulfidation. The results were discussed using the recently developed concept of interlayer dynamics of the active sites of the CoMoS phase.

© 2014 Elsevier B.V. All rights reserved.

1. Introduction

Production of clean fuels with less than 10 ppm sulfur content is one of the most important and claiming the attention problem in recent petroleum refinery [1]. The countermeasures for the ultra deep desulfurization are to apply novel highly active catalysts, and to optimize the operation conditions of the hydrodesulfurization (HDS) process. The development and application of more active and stable catalysts could enhance the productivity and improve the product quality without negative impacts on capital investment.

It is known that the active phases of the HDS catalysts are the MoS_2 or WS_2 nanocrystallites promoted by cobalt or nickel, deposited on a high specific surface area supports [2]. These active phases are obtained through the sulfidation of an oxidic precursor prepared by incipient wetness impregnation of a γ -alumina with

an aqueous solution containing the elements to be deposited, followed by drying and calcinations steps. Catalytic properties of HDS catalysts depend on various factors and their combinations (composition of active phase precursors, support, preparation conditions and others).

Activation procedure such as sulfidation is an important step to improve catalytic properties of sulfide catalysts. Investigation of sulfidation mechanism of various HDS catalysts was studied in detail with the 70-ies of the last century. Two different routes are commonly used for sulfidation of HDS catalysts [2]: (1) with a $\text{H}_2/\text{H}_2\text{S}$ mixture, carried out in gas phase and most practiced in laboratory experiments, and (2) with spiked feedstock, in which sulfidation is mainly done by the sulfur of the organosulfide agents (also called "spiking" agents). Industrially, fresh oxidic catalysts are activated by addition of sulfur-containing compounds like CS_2 , dimethyldisulfide (DMDS) or polysulfides to the feedstock [3–8]. It is known that conversion of the oxidic catalyst structure into the sulfided phase during gas or liquid phase sulfidation methods determines the final structure and performance of the catalyst

* Corresponding author. Tel.: +7 846 242 3580; fax: +7 846 242 3580.
E-mail address: P.A.Nikulshin@gmail.com (P.A. Nikulshin).

[5–10]. There is no consensus on which of sulfidation method is better. Thus for new precursors and HDS catalysts it is necessary to investigate both sulfidation methods.

Nowadays heteropolycompounds (HPCs) as precursors of an active phase of HDS catalysts attract special attention of researchers [11–33]. Catalytic properties strongly depend on the nature of the starting HPCs used for the preparation of the oxide precursors. The main advantage of HPCs of Anderson type is the presence of a 3 *d*-metal (Ni and Co included) as a heteroatom in heteropolyanion (HPA) [16–18,23–27]. Such metal plays the role of a promoter in the formation of the catalyst active phase and its nature is extremely important for catalytic activity [17]. The proximity of cobalt and molybdenum atoms in starting material has been considered by van Veen et al. [34] as a criterion for obtaining good promoting effects of the Co atoms. The use of HPAs with higher Co/Mo ratio than in Anderson type XMo_6HPA leads to enhance of the promoting effect of the cobalt in the HDS of thiophene [16,17,20,21,24,30,31]. However, a HPA, with Co/Mo ratio equal 0.5 is not found yet. It has been established [20,21,30,31] that catalysts prepared from Co (Ni) salts of HPAs are more effective than synthesized from ammonium salts or from ammonium heptamolybdate with cobalt nitrate by conventional methods. Because of different reactivity, sulfidation mechanism of Co^{2+} cations in cobalt salt of $[\text{Co}_2\text{Mo}_{10}\text{O}_{38}\text{H}_4]^{6-}$ ($\text{Co}_3\text{-Co}_2\text{Mo}_{10}\text{HPA}$) may be distinguished from Co^{3+} placed into $\text{Co}_2\text{Mo}_{10}\text{HPA}$ [20]. We have assumed that the use of $\text{Co}_3[\text{Co}_2\text{Mo}_{10}\text{O}_{38}\text{H}_4]$ salt as catalyst precursor does not provide with required molecular contact of Co^{2+} with HPA on the surface of the carrier, especially at drying, calcination and sulfidation stages [35]. Simultaneous use of $\text{Co}_2\text{Mo}_{10}\text{HPA}$ and Co complexes with chelating agents (citric acid (hereafter CA) or tartaric acid) resulted in the formation of more active catalysts than ones prepared on the basis of $\text{Co}_3[\text{Co}_2\text{Mo}_{10}\text{O}_{38}\text{H}_4]$ [35–37].

The objective of the research was to study sulfidation mechanisms of the HDS catalysts prepared with the use of $\text{Co}_2\text{Mo}_{10}\text{HPA}$ and cobalt citrate. We attempted to understand how sulfidation of $\text{Co}_2\text{Mo}_{10}\text{HPA}$ based catalysts occurred and to establish a possible difference between sulfidation of Co atoms from cobalt citrate and $\text{Co}_2\text{Mo}_{10}\text{HPA}$. Further on, we studied how the sulfidation method (by the gas or liquid phase) influences the active phase and catalytic properties (activity and stability) of the sulfidized catalysts in diesel hydrotreating (HDT) process. We considered possible catalyst deactivation mechanisms in view of recently developed concept of interlayer dynamics paying special attention to cobalt stability on the particle edges of MoS_2 crystallites [38,39].

2. Experimental

2.1. Preparation of catalysts

The ammonium salt of decamolybodicobaltate heteropolyacid (III) $(\text{NH}_4)_6[\text{Co}_2\text{Mo}_{10}\text{O}_{38}\text{H}_4] \cdot 7\text{H}_2\text{O}$ ($\text{Co}_2\text{Mo}_{10}\text{Am}$) was synthesized in accordance with published procedures [40,41]. To confirm the composition and structure of the heteropolycompound, its elemental analysis, IR spectrum and phase composition were determined [23]. Decamolybodicobaltate heteropolyacid $\text{H}_6[\text{Co}_2\text{Mo}_{10}\text{O}_{38}\text{H}_4]$ (here in $\text{Co}_2\text{Mo}_{10}\text{HPA}$) was prepared by cation exchange of NH_4^+ using KU-2 \times 8 sulfocation exchanger in H^+ form (Ural Chemical Company, Russia) [40,41]. For this purpose, a water solution of $\text{Co}_2\text{Mo}_{10}\text{Am}$ with concentration of Mo equal to 0.65 mol/l is fed into the tube reactor loaded with 300 cm^3 of KU-2 cation exchanger in H^+ form at room temperature and flow rate of $150\text{ cm}^3/\text{h}$. The exchange degree was controlled by reaction with 12-molybophosphoric acid and using Raman spectroscopy method. Solid $\text{Co}_2\text{Mo}_{10}\text{HPA}$ was obtained by water distillation in vacuum

Table 1
Properties of SRGO, LCO and LCGO used for hydrotreating.

Item	SRGO	LCO	LCGO
Density at 20 °C (g/cm ³)	0.844	0.898	0.858
Total sulfur content (wt.%)	1.04	1.29	1.51
Total nitrogen content (ppm)	134	422	1120
Total aromatic content (wt.%)	26.5	51.1	35.7
Mono-aromatics (wt.%)	20.0	33.4	25.0
Bi-aromatics (wt.%)	5.5	15.2	9.1
Tri-aromatics (wt.%)	1.0	2.5	1.6
Iodine number, J_2 g/100 g	1	6	50
Flash point (°C)	62	64	61
Distillation (°C)			
IBP	170	170	154
10 vol.%	224	190	181
50 vol.%	278	253	265
90 vol.%	336	330	351
95 vol.%	350	340	364
FBP	362	355	378

rotary evaporator at 50–60 °C. Composition of $\text{Co}_2\text{Mo}_{10}\text{HPA}$ was confirmed by elemental analysis and Raman spectroscopy.

The $\text{Co}_3(\text{CA})_{4.5}\text{-Co}_2\text{Mo}_{10}/\text{Al}_2\text{O}_3$ catalyst was prepared by wet incipient pore-volume impregnation of the γ -alumina extrudates (specific surface area $203\text{ m}^2/\text{g}$, pore volume $0.7\text{ cm}^3/\text{g}$ and effective pore radius 62.2 \AA) with aqueous solutions containing the required amounts of CoCO_3 , $\text{Co}_2\text{Mo}_{10}\text{HPA}$ and citric acid monohydrate (here in CA). The preparation procedure was as follows. CoCO_3 , CA and $\text{Co}_2\text{Mo}_{10}\text{HPA}$ (with Co/CA mole ratio = 1:1.5) were added to ion-exchanged water followed by heating up to 50 °C and stirring to prepare impregnation solution. Then the alumina extrudates were immersed in the impregnation solution. The resulting catalyst was air-dried at room temperature for 24 h, at 60 °C for 2 h, at 80 °C for 2 h and at 110 °C during 5 h, without calcination.

For comparison purposes, the second catalyst of the $\text{Co}_2\text{Mo}_{10}/\text{Al}_2\text{O}_3$ formula was prepared by wet incipient pore-volume impregnation of the alumina with the $\text{Co}_2\text{Mo}_{10}\text{Am}$ solution required concentration. The preparation procedure and treatment conditions were equal as the $\text{Co}_3(\text{CA})_{4.5}\text{-Co}_2\text{Mo}_{10}/\text{Al}_2\text{O}_3$ catalyst.

The elemental analysis (Mo and Co) was performed by a EDX800HS analyzer after calcination of catalyst probe at 550 °C for 2 h. Mo content was equal to 10 wt.% for both catalysts; Co content was equal to 3.0 wt.% in the $\text{Co}_3(\text{CA})_{4.5}\text{-Co}_2\text{Mo}_{10}/\text{Al}_2\text{O}_3$ catalyst and 1.3 wt.% in the $\text{Co}_2\text{Mo}_{10}/\text{Al}_2\text{O}_3$.

2.2. Sulfidation of catalysts

2.2.1. Gas phase sulfidation of catalysts

Both catalysts were subjected to gas phase sulfidation. For this purpose, catalyst samples were placed into a separate glass reactor where sulfidizing process was carried out under a flowing $\text{H}_2/\text{H}_2\text{S}$ mixture (85/15 v/v %, 50 ml/min, 0.1 MPa) at 20, 100, 200, 300 and 400 °C for 1 h. Samples were then cooled down to room temperature at a rate of 20–25 °C/min under the reactive mixture. The sulfided catalysts were transferred into glass vials under organic solvent in order to avoid any contact with air. The nomenclature of the gas phase sulfidized samples will be the same as the oxidic one with the supplementary extension–GS-T, where “T” is the final sulfidation temperature.

2.2.2. Liquid phase sulfidation of catalyst

Liquid phase sulfidation was carried out in bench-scale flow reactor for the $\text{Co}_3(\text{CA})_{4.5}\text{-Co}_2\text{Mo}_{10}\text{HPA}/\text{Al}_2\text{O}_3$ catalyst. Straight run gas oil (SRGO) with DMDS (2 wt.%) was used as a feedstock. The characteristics of the SRGO are presented in Table 1. The catalysts were soaked with this sulfiding feed in hydrogen atmosphere

(3.5 MPa) at 140 °C, using a liquid hourly space velocity (LHSV) of 4 h⁻¹. Then the LHSV was decreased to 2 h⁻¹ (with H₂/oil (HTO)=300 NL/L) and the bed temperature was raised to 230 °C at a rate of 25 °C/h and stabilized for 8 h. The final temperature of sulfidation was 340 °C (ramping rate of 20 °C/h) and it was stabilized for 9 h. In each sulfidation experiment catalyst sample was cooled down to room temperature at a rate of 15–20 °C/min under the reactive mixture and an organic solvent. Different parameters of liquid phase sulfidation (temperature and duration) were chosen after full sulfidation program has been carried out with controlling H₂S concentration in gas phase. The sulfided catalysts were also transferred into glass vials under an organic solvent in order to avoid any contact with air. The nomenclature of the liquid phase sulfidized samples will be the same as the oxidic one with the supplementary extension–LS-T/t, where “T” corresponds to final sulfidation temperature and “t” is duration at that.

2.3. Characterization of catalysts

2.3.1. Textural properties of catalysts

Textural characteristics of the prepared carriers and catalysts were determined by nitrogen adsorption at 77 K on a Quantachrome Autosorb-1 adsorption porosimeter. Specific surface area was calculated using Brunauer–Emmett–Teller method at relative partial pressure P/P₀ of 0.05–0.3. Total pore volume and pore size distribution were determined by a desorption curve using the Barret–Joyner–Halenda model at relative partial pressure P/P₀ of 0.99. The samples were vacuum-dried before adsorption measurement at 110 °C for 6 h.

2.3.2. Thermogravimetric analysis

Thermal analysis, the thermogravimetric (TG) and differential thermogravimetric (DTG) analysis of spent samples were conducted using a NETZSCH STA 4449 F3 Jupiter apparatus. TG and DTG curves were recorded in flowing air in the range from room temperature to 600 °C (heating rate 10 °C/min). For analysis, 20 mg of a sample was loaded in a corundum crucible, calcined alumina was being used as a reference sample.

2.3.3. High-resolution transmission electron microscopy (HRTEM)

HRTEM images of the catalysts were obtained on a Tecnai G2 20 electron microscope with a lattice-fringe resolution of 0.14 nm at an accelerating voltage of 200 kV. The high-resolution images of periodic structures were analyzed by Fourier method. Local energy-dispersive X-ray analysis (EDX) was carried out on an EDAX spectrometer (EDAX Co) fitted with Si (Li) detector with resolution of 130 eV. The samples examined by HRTEM were prepared on perforated carbon film mounted on a copper grid. The 10–15 most representative micrographs were taken for each catalyst and geometric properties such as average slab length and the stacking number were measured manually. Typically, the lengths of at least 400 slabs were measured for each catalyst. As a measure for the CoMoS₂ dispersion, the average fraction of Mo atoms at the MoS₂ edge surface, denoted as D, was calculated assuming that these MoS₂ slabs are present as perfect hexagons [42,43]. This approach was used earlier for promoted CoMoS₂ active phase [44,45]. The MoS₂ dispersion (D) is statistically evaluated by dividing the total number of Mo atoms at the edge surface by the total number of Mo atoms using the slab sizes determined from the TEM micrographs,

$$D = \frac{\sum_{i=1..t} 6n_i - 6}{\sum_{i=1..t} 3n_i^2 - 3n_i + 1}, \quad (1)$$

with n_i being the number of Mo atoms along one side of a MoS₂ slab determined from its length and t being the total number of slabs shown by the TEM micrographs. Furthermore, the number of slabs

per stack was determined, resulting in an average stacking degree (\bar{N}) calculated by

$$\bar{N} = \frac{\sum_{i=1..t} n_i N_i}{\sum_{i=1..t} n_i}, \quad (2)$$

with n_i the number of stacks with N_i layers.

2.3.4. X-ray photoelectron spectroscopy (XPS)

The samples of the sulfided catalysts were analyzed by XPS. The spectra were measured on a Kratos Axis Ultra DLD spectrometer using a monochromatic AlK source (hν = 1486.6 eV, 150 W). The binding energy scale of the spectrometer was preliminarily calibrated by the position of the peaks of Au 4f_{7/2} (83.96 eV) and Cu 2p_{3/2} (932.62 eV) core levels for pure gold and copper metals. The samples were mounted on a holder using double sided adhesive tape. For non-conductive samples the Kratos charge neutralizer system was used and the spectra were charge corrected to give the C 1s spectral component of adventitious carbon (C–C, C–H) a binding energy of 284.8 eV. In addition to the survey photoelectron spectra, more narrow spectral regions (Al 2p, S 2p, S 2s + Mo 3d, C 1s, O 1s and Co 2p) were recorded. The pass energy of the analyzer was 160 eV for the survey spectra and 40 eV for the narrow scans. Analysis of the individual spectral regions allowed determining the values of binding energies of the peaks, identifying the chemical state of the elements, as well as calculating the ratios of the atomic concentrations of the elements on the catalyst surface.

The collected spectra were analyzed by using CasaXPS software, Version 2.3.16 after applying a Shirley background subtraction and Gaussian (30%)–Lorentzian (70%) decomposition parameters. The decomposition of the S 2p, Mo 3d and Co 2p XPS spectra were performed using the appropriate oxide and sulfided references as supported monometallic catalysts and the methodology for the decomposition of CoMo/Al₂O₃ spectra set up by Gandubert et al. [46,47].

Examples of spectra decomposition are reported in Fig. 1. The XPS decomposition led to the quantification of the absolute amount of each species as follows:

$$[j] = \frac{A_j / S_j}{\sum_{i=1..n} A_i / S_i} \times 100\%, \quad (3)$$

where A_i is the measured area of the species i, S_i is the sensitivity factor of the atom related to the species i (furnished by the manufacturer) and [j] is the absolute amount of the species j.

We determined the relative concentrations of each species, Co²⁺, Co₉S₈, CoMoS, Mo⁶⁺, MoS_xO_y and MoS₂, for all the sulfided catalysts. For example, the relative amount of the CoMoS phase was determined by using the following equation:

$$\text{CoMoS} = \frac{A_{\text{CoMoS}}}{A_{\text{CoMoS}} + A_{\text{Co}_9\text{S}_8} + A_{\text{Co}^{2+}}} \times 100\%, \quad (4)$$

where A_X represents the peak area of the species (X).

Effective Co content in CoMoS phase was determined using the equation:

$$C(\text{CoMoS}) = \text{CoMoS} \times [\text{Co}], \quad (5)$$

where [Co] represents the effective concentration of cobalt determined by XPS, wt.%.

The promoter ratio was determined using the following equation:

$$(\text{Co}/\text{Mo})_{\text{slab}} = \frac{C_{\text{CoMoS}}}{C_{\text{MoS}_2}}, \quad (6)$$

where C_X is absolute concentration of Co (Mo) in CoMoS (MoS₂) species, at.%.

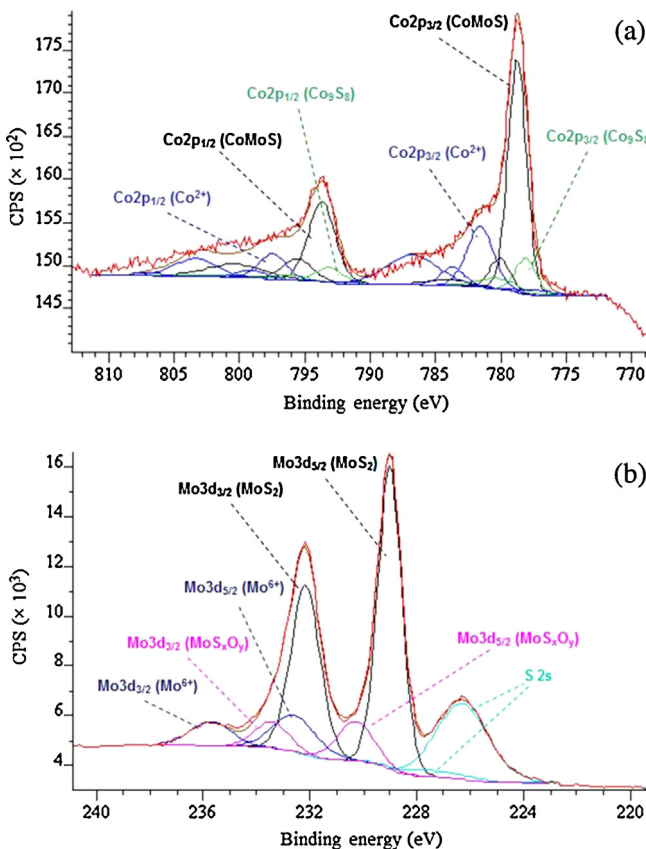


Fig. 1. XPS Co 2p (a) and Mo 3d (b) spectra of the $\text{Co}_3(\text{CA})_{4.5}\text{-Co}_2\text{Mo}_{10}/\text{Al}_2\text{O}_3$ catalyst; for (a) in blue: Co^{2+} oxide contributions; in green: Co_9S_8 contributions; in black: CoMoS phase contributions; for (b) in blue: Mo^{6+} oxide contributions; in pink: MoS_xO_y contributions; in black: MoS_2 contributions. (For interpretation of the references to color in this figure legend, the reader is referred to the web version of the article.)

The absence of any signal at 169.0 eV (characteristic of sulfates) indicates that no reoxidation of the sulfided catalysts occurred during the transfer of the solid from the sulfiding reactor to the XPS machine.

2.4. Catalytic performances

The synthesized catalysts were tested in a bench-scale flow reactor unit in the process of hydrotreating (HDT) of mixture of 70 wt.% SRGO with 16 wt.% light cycle oil (LCO) and 14 wt.% light coker gas oil (LCGO). Characteristics of the feedstocks are presented in Table 1. The system contained units for specifying, maintaining, and controlling the temperature, pressure, and hydrogen-containing gas and feed flow rates. The reactor temperature, pressure, feed and hydrogen flow rates were maintained within $\pm 1^\circ\text{C}$, ± 0.05 MPa, ± 0.1 mL/h, and 0.2 L/h, respectively. 10 cm³ of catalyst sample (pellet size of 0.25–0.55 mm) was diluted with low surface area carborundum (0.04–0.06 mm) in a 1:1 ratio (catalyst:SiC) for minimizing heat and mass transfer limitations [48]. Before the testing, the catalyst samples were activated by gas or liquid phase method. Gas phase sulfidation was carried out with a mixture of 15% H_2S in H_2 (50 ml/min) at 400 °C and 0.1 MPa for 2 h. Liquid phase sulfidation was performed using the procedure described in par. 2.2.2 with duration at 230 °C for 8 h and 340 °C for 9 h.

The tests were performed under the following conditions: temperature of 340–370 °C; pressure of 3.5–4.0 MPa; LHSV of 1.5–2.0 h⁻¹; HTO of 150–500 NL/L. After sulfidation of catalysts, SRGO was first used as a feedstock during 30 h in the working

conditions for aging of the catalyst. Then mixed feedstock was applied. Four sequential regimes were used for determining catalyst properties. The first regime (denoted as T1) was carried out in the following conditions: $T = 355^\circ\text{C}$, $P = 4.0$ MPa, LHSV = 1.5 h⁻¹, HTO = 500 NL/L for 20 h. Then in second regime (denoted as T2) we changed conditions to better distinguish activity of the catalysts: $T = 340^\circ\text{C}$, $P = 3.5$ MPa, LHSV = 2.0 h⁻¹, HTO = 350 NL/L. After that, accelerated deactivation (denoted as AD) at $T = 370^\circ\text{C}$, $P = 1.0$ MPa, LHSV = 2.0 h⁻¹, HTO = 150 NL/L for 50 h was carried out. Conditions of final regime (denoted as T3) were equal to T2.

Sulfur content in hydrogenated products was used as a measure of catalyst activity. The total sulfur content in the feedstock and products was determined on a Shimadzu EDX800HS analyzer. We also estimated deactivation degree (D_d) using the equation:

$$D_d = \left(\frac{S_p^{\text{After AD}} - S_p^{\text{Before AD}}}{S_p^{\text{Before AD}}} \right) \times 100\%, \quad (7)$$

where $S_p^{\text{After AD}}$ is steady-state sulfur content in product obtained in regime T3 after accelerated deactivation (ppm), $S_p^{\text{Before AD}}$ is steady-state sulfur content in product obtained in regime T2 before accelerated deactivation (ppm).

The coke content in spent catalysts was determined by quantitative oxidation to CO_2 followed by GC analysis.

3. Results

3.1. Evolution of the $\text{Co}_2\text{Mo}_{10}/\text{Al}_2\text{O}_3$ and the $\text{Co}_3(\text{CA})_{4.5}\text{-Co}_2\text{Mo}_{10}/\text{Al}_2\text{O}_3$ catalysts during gas phase sulfidation

Textural characteristics of the $\text{Co}_2\text{Mo}_{10}/\text{Al}_2\text{O}_3$ catalyst were changed during its sulfidation (Table 2). Specific surface area of the $\text{Co}_2\text{Mo}_{10}/\text{Al}_2\text{O}_3$ catalyst decreased linearly from 138 to 106 m²/g, pore volume decreased from 0.49 to 0.38 cm³/g and only average pore radius was approximately constant.

On the contrary, specific surface area and pore volume of the $\text{Co}_3(\text{CA})_{4.5}\text{-Co}_2\text{Mo}_{10}/\text{Al}_2\text{O}_3$ catalyst increased from 118 to 180 m²/g and from 0.38 to 0.45 cm³/g during gas phase sulfidation. Thus, the use of cobalt citrate for preparation of HDS catalyst significantly influenced on its textural characteristics after sulfidation. It should be mentioned that increased surface area and pore volume was due to contribution from deposited microporous carbon residues [37,49].

The chemical species present on the surface of the precursors and sulfided samples were evaluated by XPS. Fig. 2 shows Mo 3d and Co 2p XPS spectra of the $\text{Co}_2\text{Mo}_{10}/\text{Al}_2\text{O}_3$ catalysts obtained by gas phase sulfidation at various temperatures. The Mo spectra exhibit a Mo 3d_{5/2} peak at 228.8 eV characteristic of MoS_2 , while there is a Co 2p_{3/2} peak at about 778.6 eV in the Co spectra characteristic of Co in a sulfur environment. A peak at binding energy (BE) 226.1 eV is assigned to sulfur (S 2s). In S 2p spectra a peak at BE = 161.6 ± 0.1 eV is characteristic of sulfides containing sulfur as S^{2-} . The binding energies of the main contributions are reported in Table 1S and are in good agreement with the values reported in the literature [47,50–54]. According to Topsøe with co-workers [52], the binding energy differences BE (Co2p_{3/2})–BE (S2p) and BE (Co2p_{3/2})–BE (Mo3d_{5/2}) are characteristic for Co atoms in CoMoS phase. Table 2S reports the binding energy differences characteristic of the CoMoS phase between the main Co 2p_{3/2}, Mo 3d_{5/2} and S 2p_{3/2} transitions.

Sulfidation of the $\text{Co}_2\text{Mo}_{10}/\text{Al}_2\text{O}_3$ catalyst begins from room temperature because in Mo 3d and Co 2p spectra signals corresponding to sulfide species emerge and intensities of the peaks of the oxide states of Co and Mo decrease. At high temperature of sulfidation the character of Mo 3d spectra undergoes almost no change but sulfidation of the Co atoms ends at 400 °C.

Table 2

Textural properties of the $\text{Co}_2\text{Mo}_{10}/\text{Al}_2\text{O}_3$ and the $\text{Co}_3(\text{CA})_{4.5}-\text{Co}_2\text{Mo}_{10}/\text{Al}_2\text{O}_3$ catalysts after gas phase sulfidation at different temperatures and liquid phase sulfidation at chosen parameters.

Catalyst	Specific surface area (m^2/g)	Pore volume (cm^3/g)	Average pore radius (\AA)
$\text{Co}_2\text{Mo}_{10}/\text{Al}_2\text{O}_3\text{-Ox}^{\text{a}}$	138	0.49	61.9
$\text{Co}_2\text{Mo}_{10}/\text{Al}_2\text{O}_3\text{-GS-20}^{\text{b}}$	125	0.43	61.9
$\text{Co}_2\text{Mo}_{10}/\text{Al}_2\text{O}_3\text{-GS-100}$	109	0.39	62.0
$\text{Co}_2\text{Mo}_{10}/\text{Al}_2\text{O}_3\text{-GS-200}$	103	0.39	62.0
$\text{Co}_2\text{Mo}_{10}/\text{Al}_2\text{O}_3\text{-GS-300}$	105	0.39	61.8
$\text{Co}_2\text{Mo}_{10}/\text{Al}_2\text{O}_3\text{-GS-400}$	106	0.38	61.7
$\text{Co}_3(\text{CA})_{4.5}-\text{Co}_2\text{Mo}_{10}/\text{Al}_2\text{O}_3\text{-Ox}$	118	0.38	61.9
$\text{Co}_3(\text{CA})_{4.5}-\text{Co}_2\text{Mo}_{10}/\text{Al}_2\text{O}_3\text{-GS-20}$	120	0.39	61.8
$\text{Co}_3(\text{CA})_{4.5}-\text{Co}_2\text{Mo}_{10}/\text{Al}_2\text{O}_3\text{-GS-100}$	120	0.39	61.8
$\text{Co}_3(\text{CA})_{4.5}-\text{Co}_2\text{Mo}_{10}/\text{Al}_2\text{O}_3\text{-GS-200}$	149	0.42	61.8
$\text{Co}_3(\text{CA})_{4.5}-\text{Co}_2\text{Mo}_{10}/\text{Al}_2\text{O}_3\text{-GS-300}$	159	0.41	61.8
$\text{Co}_3(\text{CA})_{4.5}-\text{Co}_2\text{Mo}_{10}/\text{Al}_2\text{O}_3\text{-GS-400}$	180	0.45	61.7
$\text{Co}_3(\text{CA})_{4.5}-\text{Co}_2\text{Mo}_{10}/\text{Al}_2\text{O}_3\text{-LS-230/0}^{\text{c}}$	114	0.39	61.2
$\text{Co}_3(\text{CA})_{4.5}-\text{Co}_2\text{Mo}_{10}/\text{Al}_2\text{O}_3\text{-LS-230/6}$	131	0.40	54.8
$\text{Co}_3(\text{CA})_{4.5}-\text{Co}_2\text{Mo}_{10}/\text{Al}_2\text{O}_3\text{-LS-275/0}$	147	0.41	53.4
$\text{Co}_3(\text{CA})_{4.5}-\text{Co}_2\text{Mo}_{10}/\text{Al}_2\text{O}_3\text{-LS-340/0}$	150	0.42	53.4
$\text{Co}_3(\text{CA})_{4.5}-\text{Co}_2\text{Mo}_{10}/\text{Al}_2\text{O}_3\text{-LS-340/4}$	165	0.44	53.2
$\text{Co}_3(\text{CA})_{4.5}-\text{Co}_2\text{Mo}_{10}/\text{Al}_2\text{O}_3\text{-LS-340/9}$	183	0.46	53.2
$\text{Co}_3(\text{CA})_{4.5}-\text{Co}_2\text{Mo}_{10}/\text{Al}_2\text{O}_3\text{-GS-400-U}^{\text{d}}$	158	0.29	61.3
$\text{Co}_3(\text{CA})_{4.5}-\text{Co}_2\text{Mo}_{10}/\text{Al}_2\text{O}_3\text{-LS-340/9-U}$	145	0.31	53.2

^a "OX" means that catalyst sample is in oxidic (initial) state.

^b "GS" means that catalyst sample was obtained by gas phase sulfidation method; for these samples last digits correspond to final sulfidation temperature (duration at different temperatures was the same and equals 1 h).

^c "LS" means that catalyst sample was obtained by liquid phase sulfidation method; for these samples last digits correspond to final sulfidation temperature and duration at this according Fig. 6.

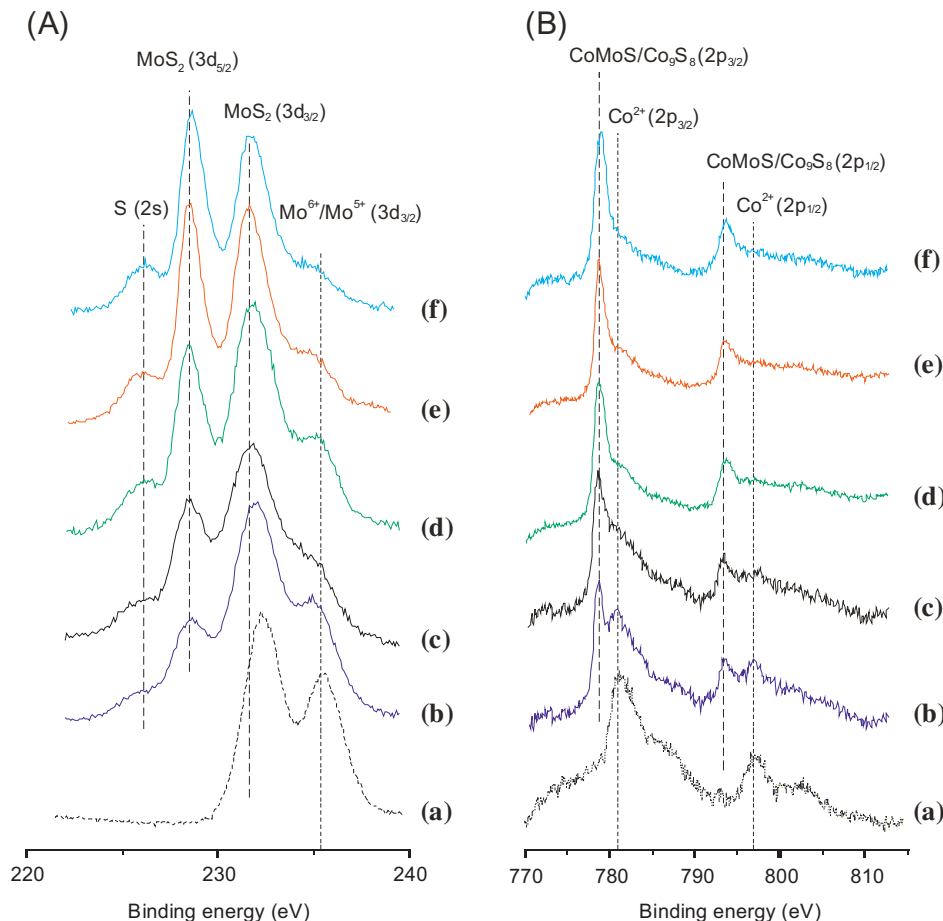


Fig. 2. XPS spectra of the $\text{Co}_2\text{Mo}_{10}/\text{Al}_2\text{O}_3$ catalyst at different stages of the gas phase sulfidation. (A) Mo 3d spectra: (a) unsulfidized, (b) $20\text{ }^\circ\text{C}$ 2 h, (c) $100\text{ }^\circ\text{C}$ 1 h, (d) $200\text{ }^\circ\text{C}$ 1 h, (e) $300\text{ }^\circ\text{C}$ 1 h and (f) $400\text{ }^\circ\text{C}$ 1 h. (B) Co 2p spectra: (a) unsulfidized, (b) $20\text{ }^\circ\text{C}$ 2 h, (c) $100\text{ }^\circ\text{C}$ 1 h, (d) $200\text{ }^\circ\text{C}$ 1 h, (e) $300\text{ }^\circ\text{C}$ 1 h and (f) $400\text{ }^\circ\text{C}$ 1 h.

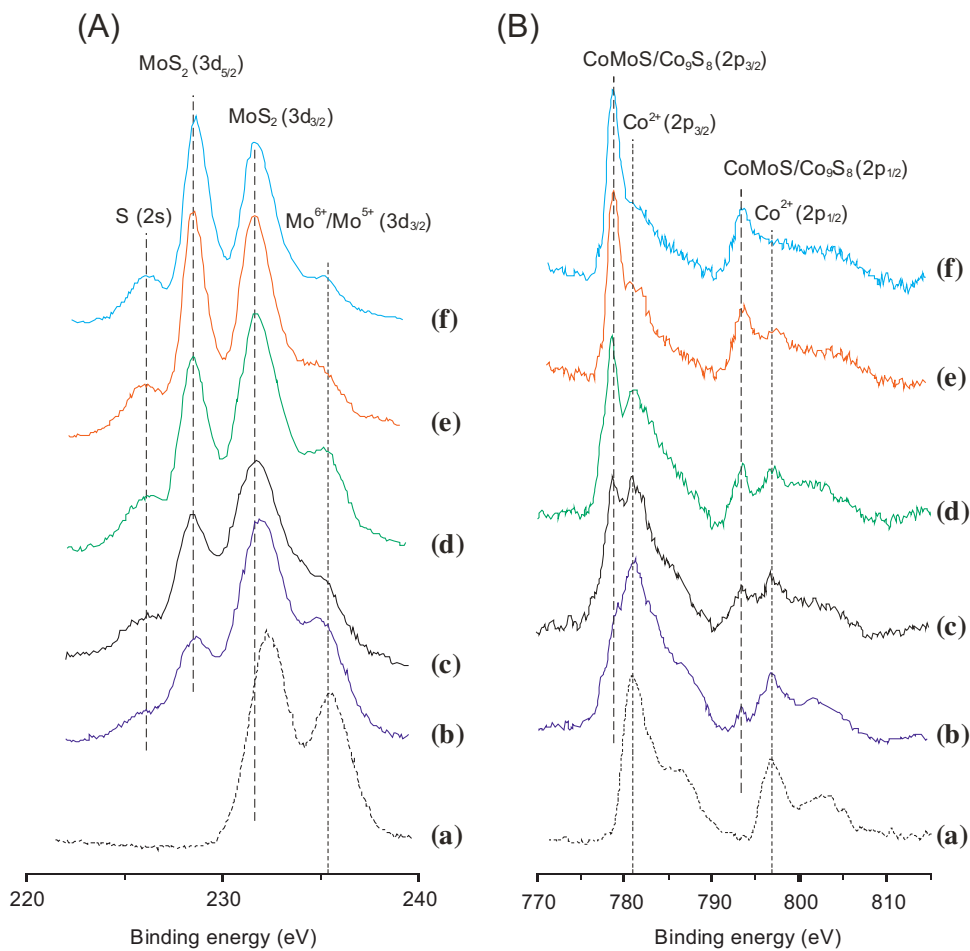


Fig. 3. XPS spectra of the $\text{Co}_3(\text{CA})_{4.5}\text{-Co}_2\text{Mo}_{10}/\text{Al}_2\text{O}_3$ catalyst at different stages of the gas phase sulfidation. (A) Mo 3d spectra: (a) unsulfided, (b) 20°C 2 h, (c) 100°C 1 h, (d) 200°C 1 h, (e) 300°C 1 h and (f) 400°C 1 h. (B) Co 2p spectra: (a) unsulfided, (b) 20°C 2 h, (c) 100°C 1 h, (d) 200°C 1 h, (e) 300°C 1 h and (f) 400°C 1 h.

Changes of XPS spectra of the $\text{Co}_3(\text{CA})_{4.5}\text{-Co}_2\text{Mo}_{10}/\text{Al}_2\text{O}_3$ catalyst during gas phase sulfidation are similar to the $\text{Co}_2\text{Mo}_{10}/\text{Al}_2\text{O}_3$ one (Fig. 3). Sulfidation of both metals starts at room temperature but most the Co atoms turn into sulfide form only at high temperature (at more than 200°C).

Decomposition of XPS spectra reveals changes of the Co and Mo species content during sulfidation of the catalysts (Table 3). In the $\text{Co}_2\text{Mo}_{10}/\text{Al}_2\text{O}_3$ catalyst the Co atoms are partially sulfidized (15%) at room temperature due to destruction of the $\text{Co}_2\text{Mo}_{10}\text{HPA}$ structure (Fig. 4), with $\text{S}/(\text{Mo} + \text{Co})$ ratio in the catalyst being equal to 1.00. Deep sulfidation of promoter atoms from the molecule of $\text{Co}_2\text{Mo}_{10}\text{HPA}$ occurs only at 300°C and above. At high sulfidation temperature (400°C) about 23% of the Co atoms remain in an oxidized state and ~2% of the Co atoms form the Co_9S_8 phase, besides, the $\text{S}/(\text{Mo} + \text{Co})$ ratio is equal to 1.97. With the sulfidation temperature increasing, the content of the Mo_{x}O_y particles passed through a maximum at 200°C . The number of the MoS_2 particles increased and reached the plateau at 300°C . Promoter ratio (Co/Mo)_{slab} was close to Co/Mo ratio in the catalyst, which indicated a high selectivity of CoMoS phase formation from this molecule (Table 3).

Similar dependences were observed in the course of the $\text{Co}_3(\text{CA})_{4.5}\text{-Co}_2\text{Mo}_{10}/\text{Al}_2\text{O}_3$ catalyst sulfidation (Fig. 4). During gas phase sulfidation the content of Co^{2+} markedly decreased at 300°C and the amount of CoMoS phase increased. However, some differences were observed: (i) the amount of CoMoS phase formed at 100°C is 29%, while at sulfidation of the $\text{Co}_2\text{Mo}_{10}/\text{Al}_2\text{O}_3$ catalyst this content reached 42%; (ii) the content of the Co_9S_8 at sulfidation of the $\text{Co}_3(\text{CA})_{4.5}\text{-Co}_2\text{Mo}_{10}/\text{Al}_2\text{O}_3$ catalyst at 400°C was 14%,

while for the $\text{Co}_2\text{Mo}_{10}/\text{Al}_2\text{O}_3$ one this parameter is no higher than 2%.

Fig. 5 shows dependence of effective amount of the Co species on temperature. The use of cobalt citrate complexes for preparation of the $\text{Co}_3(\text{CA})_{4.5}\text{-Co}_2\text{Mo}_{10}/\text{Al}_2\text{O}_3$ catalysts made it possible to double the Co effective content in the CoMoS phase in comparison with the $\text{Co}_2\text{Mo}_{10}/\text{Al}_2\text{O}_3$ sample. Besides, a promoter ratio (Co/Mo)_{slab} increased twofold and a $\text{S}/(\text{Mo} + \text{Co})$ ratio only slightly (Table 3).

3.2. Evolution of the $\text{Co}_3(\text{CA})_{4.5}\text{-Co}_2\text{Mo}_{10}/\text{Al}_2\text{O}_3$ catalyst during liquid phase sulfidation

To choose parameters for investigating liquid phase sulfidation of the $\text{Co}_3(\text{CA})_{4.5}\text{-Co}_2\text{Mo}_{10}/\text{Al}_2\text{O}_3$ catalyst, an experiment was carried out under typical liquid phase sulfidation program (for 31 h) and with controlling of H_2S content in the gas phase (Fig. 6). Two overshoots of H_2S in the gas phase gave evidence that low- and high-temperature stages of the sulfidation process had been completed. Next six liquid phase sulfidation experiments were made to study the step-by-step sulfidation process of the catalyst. In the first run a fresh catalyst was sulfidized up to 230°C . In the second, a fresh sample of the catalyst was sulfidized up to 230°C for 6 h, and so on. The complete sulfidation procedure was conducted in the sixth run.

The specific surface area and a pore volume of the $\text{Co}_3(\text{CA})_{4.5}\text{-Co}_2\text{Mo}_{10}/\text{Al}_2\text{O}_3$ catalyst during liquid phase sulfidation increased from 114 to $183\text{ m}^2/\text{g}$ and from 0.39 to $0.46\text{ cm}^3/\text{g}$, respectively (Table 2). We also found that an average pore volume decreased

Table 3

Metals partitions measured by XPS for cobalt and molybdenum species present at the surface of the $\text{Co}_2\text{Mo}_{10}/\text{Al}_2\text{O}_3$ and the $\text{Co}_3(\text{CA})_{4.5}\text{-Co}_2\text{Mo}_{10}/\text{Al}_2\text{O}_3$ catalysts after gas (liquid) phase sulfidation at different conditions and spent samples after diesel hydrotreating and accelerated deactivation processes.

Catalyst	$(\text{Co}/\text{Mo})_{\text{tot}}$	$(\text{Co}/\text{Mo})_{\text{slab}}$	$\text{S}/(\text{Mo} + \text{Co})$	Co partition (rel.%)			Mo partition (rel.%)		
				CoMoS	Co_9S_8	Co^{2+}	MoS ₂	$\text{MoS}_{\text{x}}\text{O}_{\text{y}}$	Mo^{6+}
$\text{Co}_2\text{Mo}_{10}/\text{Al}_2\text{O}_3\text{-GS-20}^{\text{a}}$	0.19	0.20	1.00	15	1	84	14	19	67
$\text{Co}_2\text{Mo}_{10}/\text{Al}_2\text{O}_3\text{-GS-100}$	0.18	0.41	1.25	43	2	56	19	29	52
$\text{Co}_2\text{Mo}_{10}/\text{Al}_2\text{O}_3\text{-GS-200}$	0.19	0.29	1.58	60	2	38	40	34	27
$\text{Co}_2\text{Mo}_{10}/\text{Al}_2\text{O}_3\text{-GS-300}$	0.20	0.19	1.69	73	2	25	78	14	9
$\text{Co}_2\text{Mo}_{10}/\text{Al}_2\text{O}_3\text{-GS-400}$	0.20	0.18	1.97	75	2	23	81	10	9
$\text{Co}_3(\text{CA})_{4.5}\text{-Co}_2\text{Mo}_{10}/\text{Al}_2\text{O}_3\text{-GS-20}^{\text{b}}$	0.49	–	1.28	15	5	80	17	18	65
$\text{Co}_3(\text{CA})_{4.5}\text{-Co}_2\text{Mo}_{10}/\text{Al}_2\text{O}_3\text{-GS-100}$	0.45	–	1.42	32	10	58	23	27	50
$\text{Co}_3(\text{CA})_{4.5}\text{-Co}_2\text{Mo}_{10}/\text{Al}_2\text{O}_3\text{-GS-200}$	0.44	0.52	1.84	48	11	41	41	32	27
$\text{Co}_3(\text{CA})_{4.5}\text{-Co}_2\text{Mo}_{10}/\text{Al}_2\text{O}_3\text{-GS-300}$	0.44	0.40	2.10	63	13	24	68	19	13
$\text{Co}_3(\text{CA})_{4.5}\text{-Co}_2\text{Mo}_{10}/\text{Al}_2\text{O}_3\text{-GS-400}$	0.45	0.37	2.12	64	14	22	77	14	9
$\text{Co}_3(\text{CA})_{4.5}\text{-Co}_2\text{Mo}_{10}/\text{Al}_2\text{O}_3\text{-LS-230/6}^{\text{c}}$	0.51	–	0.97	36	9	55	23	43	34
$\text{Co}_3(\text{CA})_{4.5}\text{-Co}_2\text{Mo}_{10}/\text{Al}_2\text{O}_3\text{-LS-275/0}$	0.52	0.84	1.27	39	13	49	24	39	37
$\text{Co}_3(\text{CA})_{4.5}\text{-Co}_2\text{Mo}_{10}/\text{Al}_2\text{O}_3\text{-LS-340/0}$	0.51	0.55	1.52	52	12	36	48	30	22
$\text{Co}_3(\text{CA})_{4.5}\text{-Co}_2\text{Mo}_{10}/\text{Al}_2\text{O}_3\text{-LS-340/4}$	0.48	0.38	1.60	52	13	35	66	20	14
$\text{Co}_3(\text{CA})_{4.5}\text{-Co}_2\text{Mo}_{10}/\text{Al}_2\text{O}_3\text{-LS-340/9}$	0.48	0.31	1.69	53	15	32	82	7	11
$\text{Co}_3(\text{CA})_{4.5}\text{-Co}_2\text{Mo}_{10}/\text{Al}_2\text{O}_3\text{-GS-400-U}^{\text{3}}$	0.45	0.29	2.01	47	28	25	74	15	11
$\text{Co}_3(\text{CA})_{4.5}\text{-Co}_2\text{Mo}_{10}/\text{Al}_2\text{O}_3\text{-LS-340/9-U}$	0.48	0.28	1.85	46	28	26	79	11	10

^a "GS" means that catalyst sample was obtained by gas phase sulfidation method; for these samples last digits correspond to final sulfidation temperature (duration at different temperatures was the same and equals 1 h).

^b "LS" means that catalyst sample was obtained by liquid phase sulfidation method; for these samples last digits correspond to final sulfidation temperature and duration at this according Fig. 6.

^c "U" means that it is spent catalyst sample obtained after diesel hydrotreating and accelerated deactivation processes.

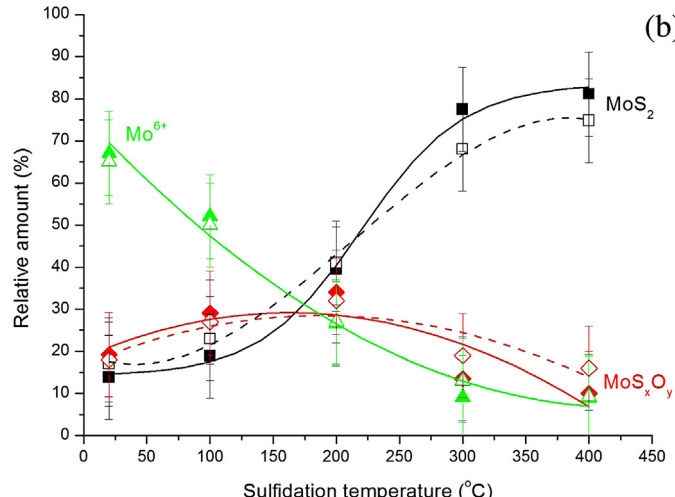
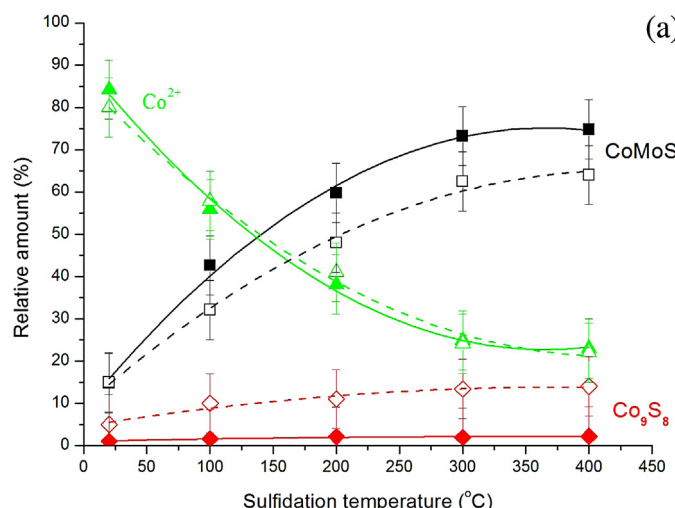


Fig. 4. Evolution of cobalt (a) and molybdenum (b) species for the $\text{Co}_2\text{Mo}_{10}/\text{Al}_2\text{O}_3$ (straight line) and the $\text{Co}_3(\text{CA})_{4.5}\text{-Co}_2\text{Mo}_{10}/\text{Al}_2\text{O}_3$ (dashed line) catalysts sulfidized by gas phase at various temperatures.

to 53.2 Å in comparison with gas phase sulfidation method (Fig. 7). These changes took place during a low-temperature stage of sulfidation process (Table 2).

XPS shows (Fig. 8) that both metals started sulfidation simultaneously with destruction of the $\text{Co}_2\text{Mo}_{10}\text{HPA}$ at low-temperature stage. Full sulfidation of both metals was reached after 6–9 h at high-temperature stage (340 °C).

Dependences of the contents of cobalt and molybdenum species on the sulfidation degree obtained during liquid phase sulfidation experiments were close to that obtained in the course of the gas phase sulfidation (Fig. 9). Formation of the CoMoS phase was occurred with higher selectivity using gas phase sulfidation method than liquid phase sulfidation. The dependence of the effective amount of the Co species on temperature is depicted in Fig. 10 and the parameters are given in Table 3. Liquid phase sulfidation led to catalyst formation with less Co content in the CoMoS phase

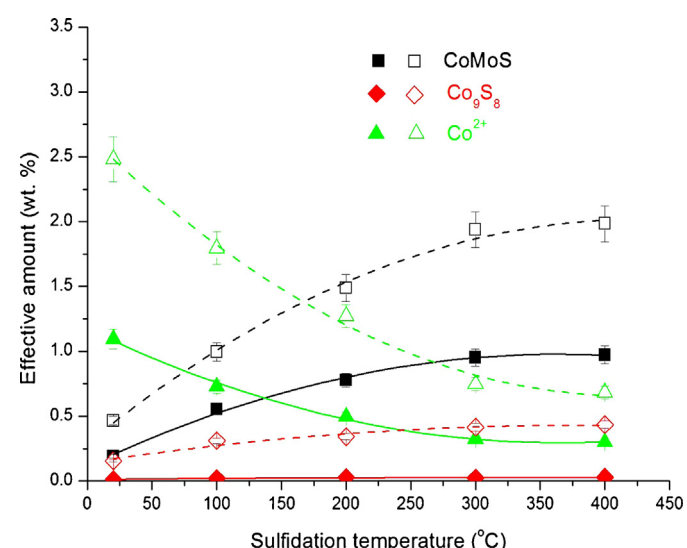


Fig. 5. Evolution of cobalt species for the $\text{Co}_2\text{Mo}_{10}/\text{Al}_2\text{O}_3$ (straight line) and the $\text{Co}_3(\text{CA})_{4.5}\text{-Co}_2\text{Mo}_{10}/\text{Al}_2\text{O}_3$ (dashed line) catalysts sulfidized by gas phase at various temperatures.

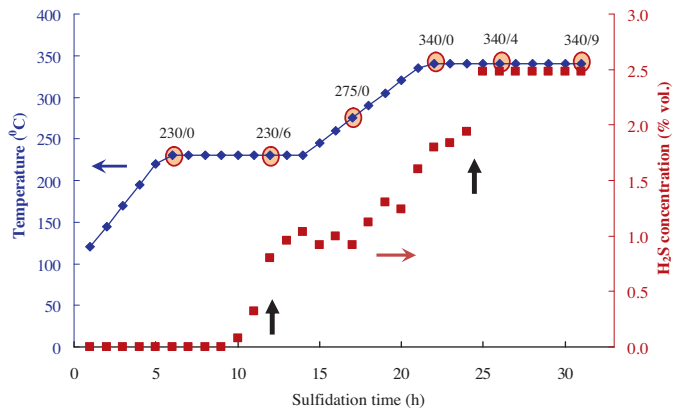


Fig. 6. Change of H_2S concentration in gas phase during liquid phase sulfidation of the $\text{Co}_3(\text{CA})_{4.5}\text{-Co}_2\text{Mo}_{10}/\text{Al}_2\text{O}_3$ catalyst. Black arrows indicate two overshoots of H_2S concentration in gas phase. Chosen conditions for studying sulfidation of catalyst are revealed by circles.

in comparison with the sample sulfided by gas phase method. Besides, the catalyst sulfided by the liquid phase had lower promoter (Co/Mo)_{slab} and $\text{S}/(\text{Mo} + \text{Co})$ ratio.

Coke content in the catalyst sulfided by the liquid phase method is higher than in the gas sulfided one. Some differences in coke composition were established by analyzing XPS C 1s spectra of the catalysts. The gas sulfided catalyst had more content of carbon with $\text{C}-\text{O}$ and $\text{C}=\text{O}$ groups than the liquid sulfided one (Fig. 11).

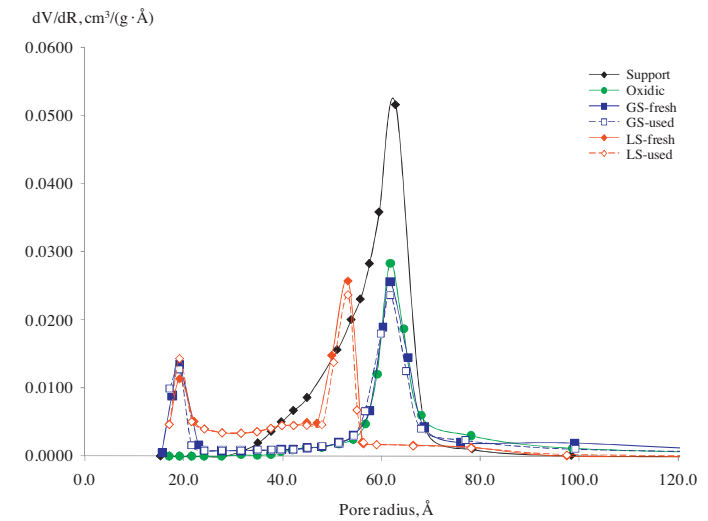


Fig. 7. Plots of pore volume distribution of alumina of catalysts sulfided by gas and liquid phase sulfidation methods and of spent samples.

The analysis of the $\text{Co}_3(\text{CA})_{4.5}\text{-Co}_2\text{Mo}_{10}/\text{Al}_2\text{O}_3$ catalyst by an HRTEM method revealed that the nuclei of the active phase were formed after ten hours of sulfidation at 230°C . They are poorly visible on the TEM images (Fig. 12) as their size is less than 10\AA . With a further increase of the temperature and time of the sulfidation,

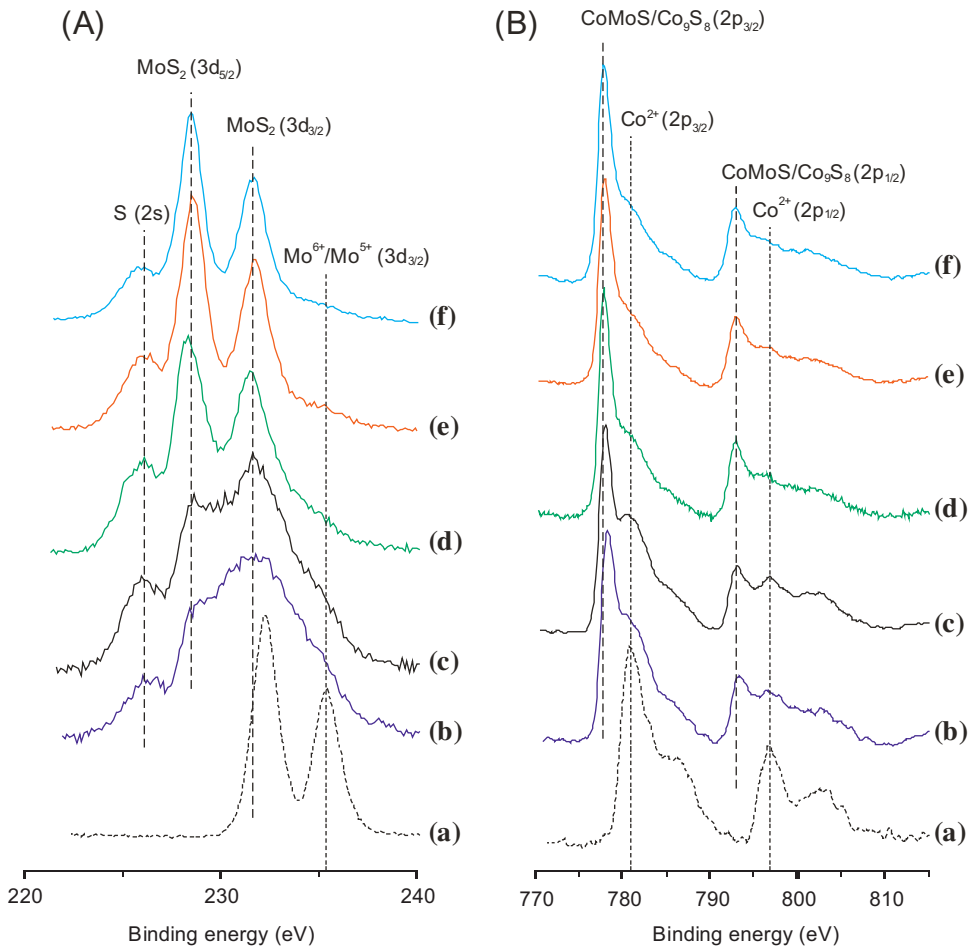


Fig. 8. XPS spectra of the $\text{Co}_3(\text{CA})_{4.5}\text{-Co}_2\text{Mo}_{10}/\text{Al}_2\text{O}_3$ catalyst at different stages of the liquid phase sulfidation. (A) Mo 3d spectra: (a) 230°C 0 h, (b) 230°C 6 h, (c) 275°C 0 h, (d) 340°C 0 h, (e) 340°C 4 h and (f) 340°C 9 h. (B) Co 2p spectra: (a) 230°C 0 h, (b) 230°C 6 h, (c) 275°C 0 h, (d) 340°C 0 h, (e) 340°C 4 h and (f) 340°C 9 h.

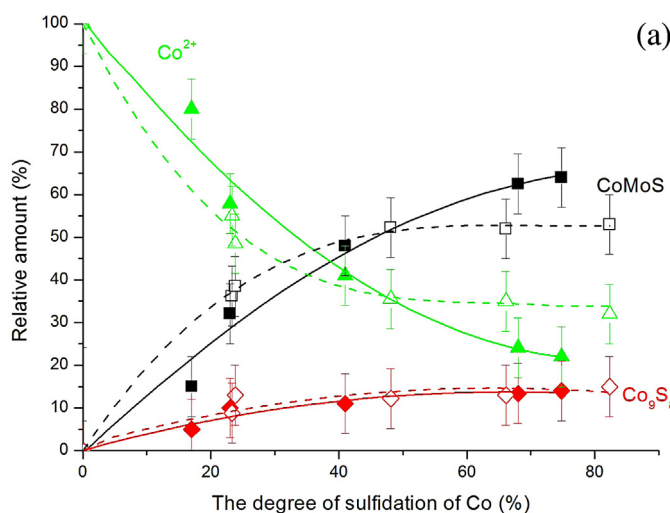


Fig. 9. Dependences of relative amount of cobalt (a) and molybdenum (b) species for the $\text{Co}_3(\text{CA})_{4.5}\text{-Co}_2\text{Mo}_{10}\text{HPA/Al}_2\text{O}_3$ catalyst on the sulfidation degree in gas phase (straight line) and liquid phase (dashed line).

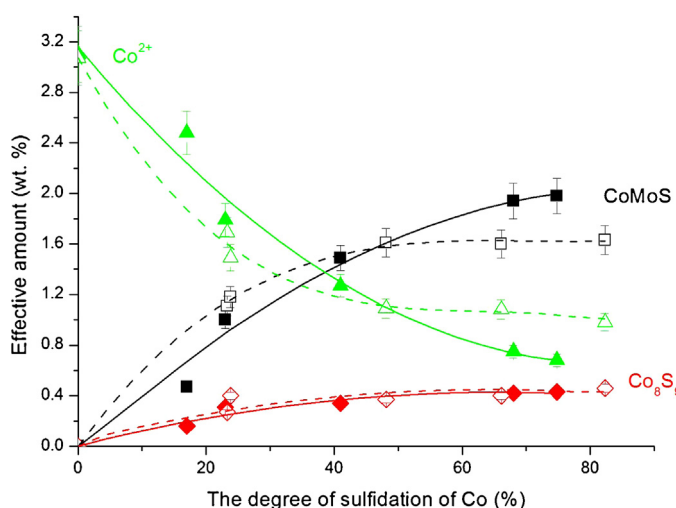


Fig. 10. Dependences of effective amount of cobalt species for the $\text{Co}_3(\text{CA})_{4.5}\text{-Co}_2\text{Mo}_{10}/\text{Al}_2\text{O}_3$ catalyst on the sulfidation degree in gas phase (straight line) and liquid phase (dashed line).

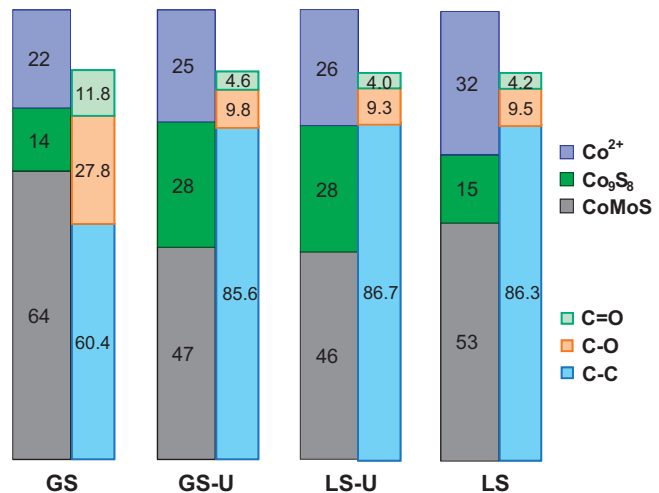


Fig. 11. XPS distributions (%) of Co and carbon species for fresh sulfided (GS and LS) and spent (GS-U and LS-U) catalysts.

there was a growth of the average stacking number of MoS_2 crystallites in active phase from 1.2 to 1.6 and average length from 2.8 to 4.5 nm. The black thread-like fringes correspond to the MoS_2 slabs. The fringes observed in the images had a spacing of about 0.65 nm which is characteristic of (002) basal planes of crystalline MoS_2 .

The active phase of the catalyst after gas phase sulfidation had the average slab length 4.2 nm and average stacking number of MoS_2 crystallites was 2.2, higher than after liquid phase sulfidation (Fig. 13, Table 4).

3.3. Investigation of catalyst properties

Results of catalytic testing are presented in Fig. 14 and Table 5. First, we determined conditions for producing hydrogenated products with sulfur content less than 50 ppm (corresponding to Euro-4 standard). The gas phase sulfidized catalyst was slightly more active. Then we used less severe conditions to distinguish catalyst activity better. Under regime T2 the difference between S content in products was 60 ppm in favor of the gas phase sulfidized sample.

AD was the next stage of catalyst testing. The conditions with a high temperature of the reactor and low hydrogen partial pressure when undesirable reactions limiting catalyst life cycle (for example, coking) took place. After that, we restored the conditions for the second measuring of the catalyst activity. After AD, the sulfur content in products obtained over both catalysts in regime T3 increased in comparison with the state before AD (T2). There was no large difference in sulfur content values in products obtained over different sulfidized catalysts at regime T3 (Table 5).

Thus, the catalyst sample sulfidized by gas phase method had better initial activity than the liquid sulfidized one, because it allowed us to produce a hydrogenated product with less S content. However, the catalyst sulfidized by liquid phase method had a lower deactivation degree during AD, i.e. it was more stable than the gas sulfidized sample (Table 5). After AD, catalyst activities of both samples were the same.

3.4. Characterization of spent catalysts

Pore volume distributions for both catalysts showed almost no change after their sulfidation (Fig. 7). The peak in the both samples with 19 Å corresponds to coke species.

Table 4

CoMoS₂ dispersion calculated from TEM micrographs of the Co₃(CA)_{4.5}-Co₂Mo₁₀/Al₂O₃ catalysts sulfided by gas and liquid phase sulfidation methods and spent samples.

Catalyst	Stacks of CoMoS ₂ per 1000 nm ²	Average length \bar{L} (nm)	Average stacking number \bar{N}	Dispersion of CoMoS ₂ D
GS	21	4.2	2.2	0.28
LS	19	4.5	1.6	0.26
GS-used	26	4.4	1.8	0.27
LS-used	24	4.4	1.6	0.27

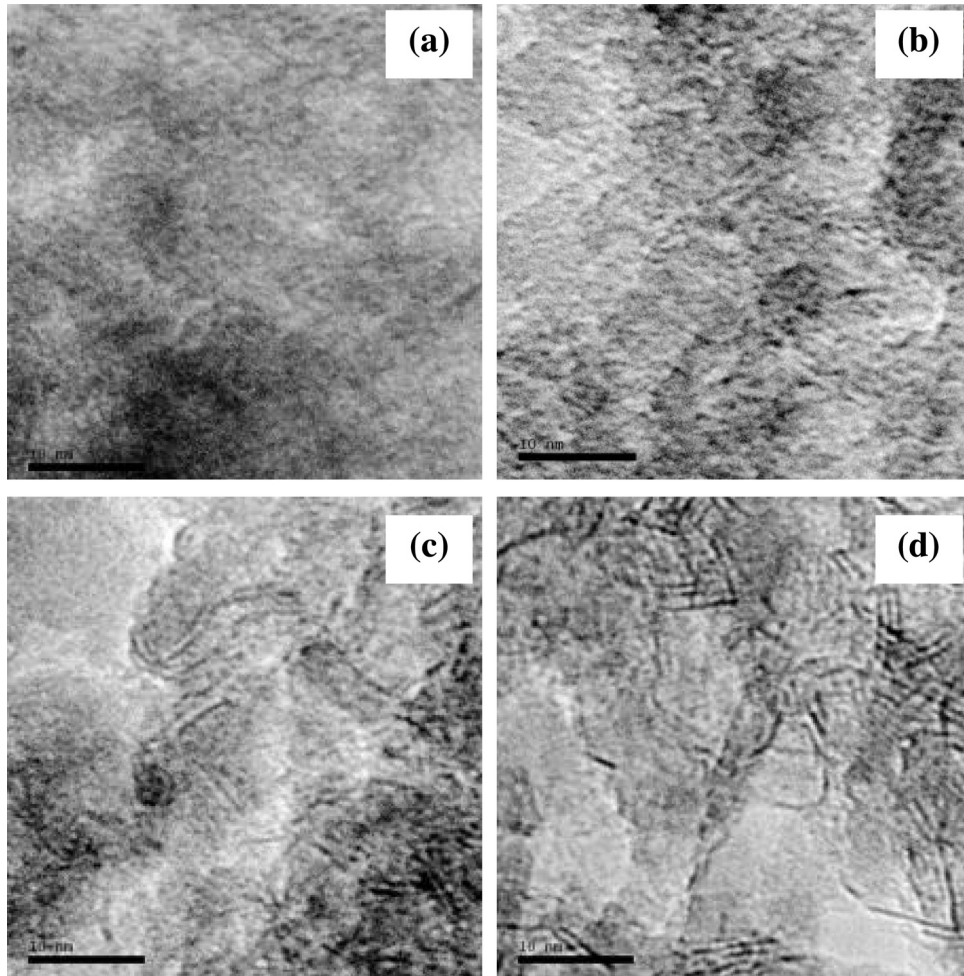


Fig. 12. HRTEM-images of the Co₃(CA)_{4.5}-Co₂Mo₁₀/Al₂O₃ catalyst sulfided by liquid phase method at different conditions: (a) 230 °C 6 h; (b) 275 °C 0 h; (c) 340 °C 0 h; (d) 340 °C 9 h.

Coke content in the spent catalysts was higher in the sample sulfided by gas phase method than the liquid phase sulfided one (Table 5). Fig. 15 shows plots of DTA of the spent catalysts. The spent catalyst sulfided by gas phase method had more exothermal effect from coke combustion because of higher coke content (Table 5). Temperature of the peak maximum was equal to 406 °C for both sample. That indirectly witnessed the similarity of coke composition in the spent samples. The XPS data confirmed this supposition because the relative carbon content in C—O and C=O groups was the same in the spent catalysts (Fig. 11).

The analysis of the spent samples by XPS showed a decrease in the (Co/Mo)_{slab} ratio for the both samples after AD (Table 3). The reduction of the Co/Mo ratio for the gas sulfided sample was more significant than that for the liquid sulfided one. Co content in CoMoS phase also decreased. Distributions of Co species in the spent catalysts were similar (Fig. 15).

Active phase morphology also changed after AD (Table 4). For the gas sulfided catalyst the changes were more marked.

4. Discussion

The differences between gas phase sulfidation of the Co₂Mo₁₀/Al₂O₃ and the Co₃(CA)_{4.5}-Co₂Mo₁₀/Al₂O₃ catalysts (Figs. 4 and 5) can be explained by different reactivity of the oxidic precursors under sulfidation conditions. It is known that a delay of sulfidation of chelating complexes of Co(Ni) used as a promoter precursor is an effective method for the preparation of highly active HDS catalysts [35,55,56]. Our results showed that the Co atoms begin to move off from citrate complexes and penetrate into the active phase at high temperatures of sulfidation whereas Co atoms from the Co₂Mo₁₀HPA begin to be sulfided together with Mo at quite low temperature. The gap between these temperatures is about 150 °C. Modification of the oxide precursors of the catalysts by cobalt citrate complexes leads to a change of sulfidation mechanism and formation of new species on the surface. During sulfidation the Co atoms from the Co-citrate migrate to the edges of multilayer slabs of CoMoS phase *in situ*

Table 5 Catalytic properties of the $\text{Co}_3(\text{CA})_{4.5}\text{-Co}_2\text{Mo}_{10}/\text{Al}_2\text{O}_3$ catalysts sulfided by gas and liquid phase sulfidation methods in HDT of blending feedstock (SRGO (70%) with LCO (16%) and LCGO (14%)).

Sulfidation method	Number of testing regime	Hydrotreating process conditions			Sulfur content in hydrogenated products (wtppm)	Deactivation degree (%)	Coke content (wt%)
		T (°C)	LHSV (h ⁻¹)	P (MPa)			
Gas phase sulfidation	T1	355	1.5	4.0	500	29	34
	T2	340	2.0	3.5	350	287	4.4
	AD	370	2.0	1.0	150	118	
	T3	340	2.0	3.5	350	384	
Liquid phase sulfidation	T1	355	1.5	4.0	500	38	14
	T2	340	2.0	3.5	350	347	
	AD	370	2.0	1.0	150	129	
	T3	340	2.0	3.5	350	396	

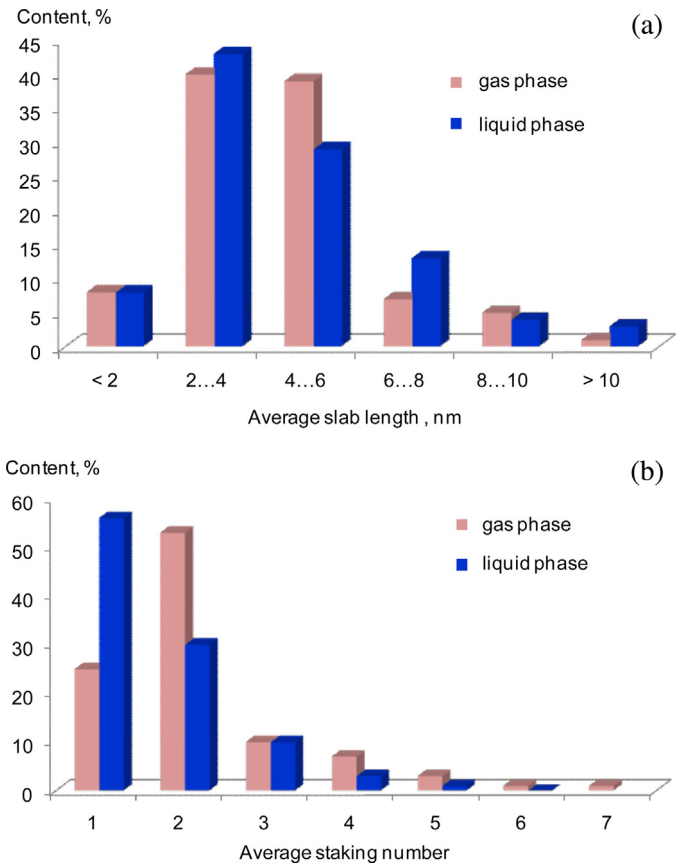


Fig. 13. Distributions of slab lengths of MoS_2 particles (a) and of stacking number of MoS_2 particles (b) for the $\text{Co}_3(\text{CA})_{4.5}\text{-Co}_2\text{Mo}_{10}/\text{Al}_2\text{O}_3$ catalyst sulfided by gas and liquid phase methods.

nascendi. Besides, some part of cobalt forms a separated cobalt sulfide phase (Fig. 4, Table 3). It was found that citrate fragments form up to 1.5 wt.% of coke [37]. This method allowed us to obtain catalyst with higher Co content in CoMoS phase equal 1.98 wt.%.

The gas phase sulfidized $\text{Co}_3(\text{CA})_{4.5}\text{-Co}_2\text{Mo}_{10}/\text{Al}_2\text{O}_3$ catalyst and oxidic sample had the same pore volume distributions (Fig. 7, Table 2). This indicates that coke and active components are located in pores filled initially by oxidic precursors. A decrease of average pore radius of catalyst at low-temperature stage of liquid phase sulfidation witnesses to coking of all the pores.

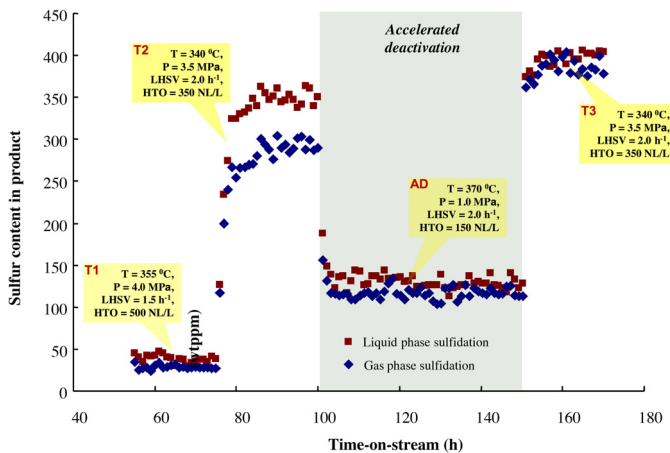


Fig. 14. Residual sulfur content in the products of HDT of mixture of SRGO (70 wt.%), LCO (16 wt.%) and LCGO (14 wt.%) over the $\text{Co}_3(\text{CA})_{4.5}\text{-Co}_2\text{Mo}_{10}/\text{Al}_2\text{O}_3$ catalysts sulfided by gas and liquid phase methods.

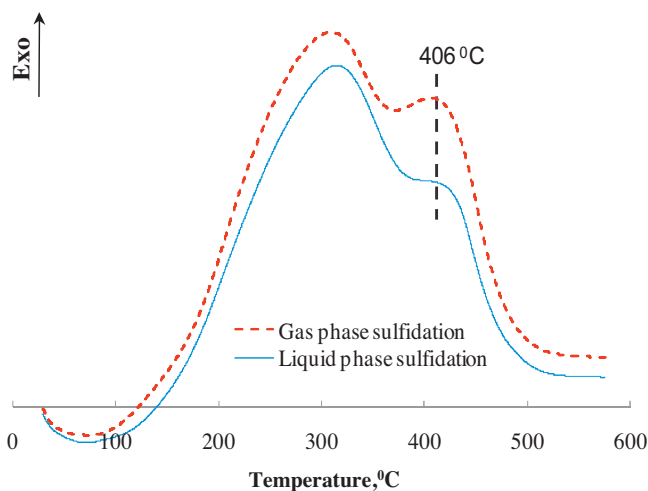


Fig. 15. Plots of DTA of the spent catalysts.

Besides, comparison of textural characteristics of the $\text{Co}_2\text{Mo}_{10}/\text{Al}_2\text{O}_3$ catalysts with the $\text{Co}_3(\text{CA})_{4.5}\text{-Co}_2\text{Mo}_{10}/\text{Al}_2\text{O}_3$ allowed us to conclude that the use of cobalt citrate complexes leads to an increase of specific surface area and pore volume (Table 2). This effect was mentioned earlier [37,49] and can be explained by the formation of coke species during the sulfidation of the catalysts containing organic additives.

The XPS and HRTEM measurements of the synthesized catalysts confirmed the formation of multilayer slabs of type II CoMoS phase after gas and liquid phase sulfidations. Fig. 16 shows the models of genesis of the active phase of the $\text{Co}_3(\text{CA})_{4.5}\text{-Co}_2\text{Mo}_{10}/\text{Al}_2\text{O}_3$ catalyst in gas or liquid phase sulfidation. Earlier [37] we found that the structure of the $\text{Co}_2\text{Mo}_{10}\text{HPA}$ is preserved after the impregnation of alumina with water solution of the precursors containing cobalt citrate. At the first step of the gas phase sulfidation the $\text{Co}_2\text{Mo}_{10}\text{HPA}$ molecules are decomposed and the framework of the next multilayered CoMoS phase was formed with Co shortage. At the second step, the destruction of cobalt citrate at higher temperatures and fixing of the Co atoms on the edges of MoS_2 crystallites took place. Thus, in the case of the gas phase sulfidation the mechanism of the active phase formation can be called as "sequential". Characteristics of the formed active phase are presented in Tables 3 and 4, Fig. 5.

In the case of the liquid phase sulfidation, the mechanism of the active phase formation differs from the gas phase method. Both metals (Co and Mo from $\text{Co}_2\text{Mo}_{10}\text{HPA}$ and Co from citrate) are sulfided simultaneously with the formation of the CoMoS II at a low-temperature stage. High-temperature sulfidation stage results in the increase of size of the CoMoS phase due to sulfidation of the Mo oxide species (Table 3, Fig. 9). Thus, the liquid phase sulfidation mechanism of the active phase formation can be called as "simultaneous". Characteristics of the formed active phase are presented in Tables 3 and 4, Fig. 10. Relative amount of MoS_2 in the catalyst subjected to gas phase sulfidation is slightly less than in the one sulfided by the liquid phase: 77% vs. 82% (Table 3). For the same particle size of MoS_2 in two different catalysts the minimal amount of particles would be in the case of the gas phase sulfidized catalyst. However, this did not happen because the gas phase sulfidized catalyst has a smaller average particle length of the active phase (Table 4) compared with the liquid phase sulfidized one, *i.e.* compensation effect takes place. In contrast, the Co content in the particles of CoMoS active phase is higher in the catalyst subjected to gas phase sulfidation than in the liquid phase: 64% vs. 53% (Table 3). The difference in the selectivity of sulfidation of Co oxide precursors is obvious. Thus, the gas phase sulfidized catalyst contains less relative content of Mo in MoS_2 but the high content of Co on the surface of

MoS_2 (CoMoS phase). Catalyst with more relative content of Mo in MoS_2 particles, but less enriched by Co atoms is formed using the liquid phase sulfidation.

The use of the gas phase sulfidation of the $\text{Co}_3(\text{CA})_{4.5}\text{-Co}_2\text{Mo}_{10}/\text{Al}_2\text{O}_3$ catalyst improves the catalyst properties (higher Co content in CoMoS phase, $(\text{Co}/\text{Mo})_{\text{slab}}$ ratio, dispersion of the active phase) comparing to the liquid sulfidation. Better formation of the CoMoS phase from these precursors in the course of the sequential sulfidation mechanism comparing to that during the simultaneous sulfidation can be explained by separate sulfidizing of the metals and hindering of the cobalt sulfidation. Sulfidation method also affects the morphology of the catalyst active phase. Partial evaporation of the liquid phase hydrocarbons could contribute to relieve exothermicity of sulfidation reaction, preventing sintering of MoS_2 slabs. Therefore the average stacking number of the liquid sulfidized catalyst is lower at 0.4 than the value for the gas sulfidized one. However, the active phase species of the liquid sulfidized catalyst is longer than species in the gas sulfidized one. The reason of this inequality is probably in the difference of the genesis mechanisms. Lower size of the active phase species of the gas sulfidized catalysts can be explained by large restraining the growth of MoS_2 crystallites by Co atoms in the sequential mechanism of the gas sulfidation process than during liquid sulfidation. More $(\text{Co}/\text{Mo})_{\text{slab}}$ ratio in gas sulfidized catalyst confirms this effect.

The gas sulfidized sample demonstrated also higher initial catalytic activity determined in T1 and T2 regimes in diesel HDT than liquid sulfidized one. It was not surprised that catalyst activity was correlated with CoMoS phase content or active sites concentration. However, after catalytic testing and AD final catalyst activity of the catalysts was approximately the same (Table 5) as the characteristics of active phase of the spent samples (Fig. 16).

Comparison of the active phase characteristics of fresh sulfidized and spent catalysts (Fig. 16, Table 5) led us to conclusion that the Co atoms escaped from the CoMoS active phase during catalyst testing and AD. Recently we showed that the Ni atoms can migrate from the NiMoS active phase under reaction conditions [38]. This process can be explained by the dynamic model [38,39]. According to the model, the neighboring layers of the multilayered MoS_2 crystallite exchange by sulfur between Mo- and S-edges placed one under another in the course of permanent reduction–sulfidation processes under hydrogen atmosphere. When the sulfur atoms bonded to the Co atoms leave the reduced edge of the layer, the atoms of the promoter also move along the sulfur atoms from one layer to an adjacent layer of higher sulfidation state. Then the process reverses. Such oscillations occur until the sulfur organic compound adsorbs on the vacancy on the reduced edge. The frequency of the oscillations determines catalytic activity of CoMoS slab. Thiophene adsorption makes transfer of a promoter to the neighboring slab improbable because the electron density of thiophene sulfur compensates the extra positive charge on the Mo atom appeared after H_2S removal. When thiophene adsorbs on the vacancy of CoMoS site the proton linked to Co moves to the SH group of the neighboring layer forming the H_2S which desorbs from this layer and new vacancy is formed. This model explains the reasons of the electron transfer from atom of promoter to Mo and different locations of the active sites responsible for HYD and desulfurization on a promoted Mo-sulfide slab. In [38] we found that blocking of the edges of MoS_2 crystallites by coke did not allow the Ni atoms to leave the places of their localization on the edges to incorporate into the structure of the adjacent layer. This led to agglomeration of promoter atoms and falling-out in the form of separated Ni particles.

Increase of the Co_9S_8 species content after deactivation of the catalysts sulfidized using either gas or liquid methods witnesses in favor of the Co atoms migration from the CoMoS to the Co_9S_8 phase (Fig. 11, Table 3). For the gas sulfidized catalyst this migration process was more intensive because Co content in CoMoS phase was

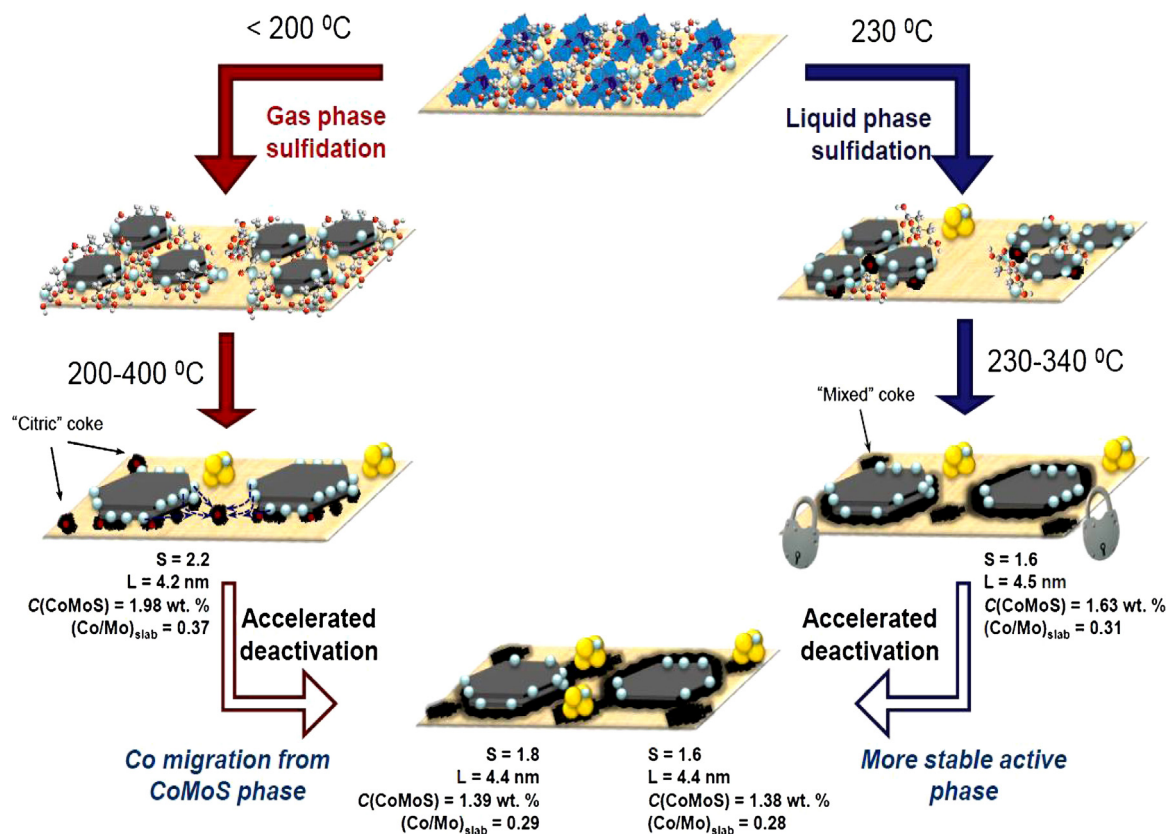


Fig. 16. CoMoS phase formation mechanisms during gas and liquid phase sulfidation of the $\text{Co}_3(\text{CA})_{4.5}-\text{Co}_2\text{Mo}_{10}/\text{Al}_2\text{O}_3$ catalyst (S —average stacking number, L —average length were found from TEM; Co content in CoMoS phase and $(\text{Co}/\text{Mo})_{\text{slab}}$ were found by XPS).

decreased from 64% to 47% and $(\text{Co}/\text{Mo})_{\text{slab}}$ ratio was decreased from 0.37 to 0.29 (Figs. 11 and 16, Table 3). In the case of the liquid sulfidized sample, these changes were occurred to a lesser degree: Co content in CoMoS phase reduced from 53% to 46% and $(\text{Co}/\text{Mo})_{\text{slab}}$ ratio decreased from 0.31 to 0.28. Thus, the liquid sulfidized sample was more resistant to the deactivation. This occurred probably due to stabilization of the active phase particles by coke formed during liquid phase sulfidation. This effect prevents Co atoms to be loosed from the CoMoS phase. It seems that coke origin in sulfidized catalysts has significant influence on their active phase morphology, catalytic properties and especially on deactivation processes. In [24] we have already shown that the use of intermediate carbon carrier placed between alumina and active phase allowed to greatly change the active phase structure and catalyst activity. Recently, other authors have indicated [54,57–60] the carbon residual species formation, when chelating agents or organic additives were used in catalysts preparation. Some residual organic fragments issued from NTA decomposition were still present on the alumina surface after sulfidation of the NTA containing catalysts at 400°C [60]. Note that these species were still observed after sulfidation followed by H_2 treatment at 250°C . These species correspond to carboxylates adsorbed on Lewis acid sites of alumina. Frizi et al. [47] used of thioglycolic acid (TGA) as an additive to improve the properties of a commercial alumina-supported CoMo catalyst. They indicated the presence of TGA carboxyl group in the metal–TGA entities after sulfidation at 350°C . The modifications of the metal–support interactions by carbon incorporation from CA on the alumina surface have been observed [59]. Thus, carbon residual species, formed from chelating agents or organic additives, reduced the interaction between the sulfide active phase and the subjacent carrier. It led to preferential formation of type II CoMoS phase and modification of the external structure of the active phase.

The coke of the catalyst sulfidized by liquid phase method did not change its composition after deactivation, *i.e.* initially was stable (Fig. 11). This coke was obtained from citrate complexes and hydrocarbon feedstock and can be called as mixed one. Coke forming in gas phase sulfidation process had only citric origin and contained some amount of C–O and C=O groups, this coke can be called as citric coke. We did not consider substitution of S atoms by C with formation of Me–C bonds because it would be thermodynamically unfavorable in activation conditions of the catalysts [61]. The oxygen-containing citric coke changed its composition during activating and testing. It became inert like coke formed in the course of liquid phase sulfidation. Moreover, the coke content increment for the gas sulfidized catalyst is higher than for the liquid sulfidized sample. These changes in coke content and composition probably induce higher mobility of the promoter atoms in the gas sulfidized catalyst. Coke species can be formed on the high active CoMo active sites and force out the promoter atoms into separate Co species. Therefore, the active sites of the gas sulfidized catalyst having higher reactivity than for the liquid sulfidized one due to higher $(\text{Co}/\text{Mo})_{\text{slab}}$ ratio, stacking number and lower average length [25,35] are more likely can be deactivated by coke species. Similar phenomenon we observed earlier [62]. Higher coke content and Co losses in spent gas sulfidized catalyst prove this hypothesis.

5. Conclusion

Mechanisms of the active phase formation from $\text{Co}_2\text{Mo}_{10}\text{HPA}$ and cobalt citrate precursors during gas and liquid phase sulfidation processes have been established. The first step of gas phase sulfidation is formation of MoS_2 nanoclusters from $\text{Co}_2\text{Mo}_{10}\text{HPA}$ with the deficiency of promoter atoms. The second step is

destruction of cobalt citrate at higher temperatures and fixing of the Co atoms on the edges of MoS_2 crystallites.

In liquid phase sulfidation, both metals (Co and Mo from $\text{Co}_2\text{Mo}_{10}\text{HPA}$ and Co from citrate) are sulfided simultaneously with the formation of nuclei of CoMoS phase II type at low temperature (230°C). At high temperature (340°C) the increase of particle size of CoMoS phase is occurred.

Gas phase sulfidation of the catalyst leads to formation of active phase with higher Co content in CoMoS and promoter ratio than liquid sulfidation. Initial activity in diesel HDT of the gas sulfided catalyst was higher than activity of the sample sulfided by the liquid phase method.

Study of behavior of the catalysts in accelerated deactivation revealed that the liquid phase sulfided sample was more resistant to the deactivation. This occurred probably due to stabilization of active phase particles by coke formed during liquid phase sulfidation. This effect prevents loss of Co atoms from CoMoS phase.

Acknowledgments

The work was financially supported by The Ministry of education and science of Russian Federation and partly by the Russian Foundation for Basic Research (grant 14-03-31901). The work was carried out on the facilities of the Multiple-Access Center "Investigation of the physicochemical properties of substances and materials" of Samara State Technical University. K.I. Maslakov acknowledges partial support from M.V. Lomonosov Moscow State University Program of Development.

Appendix A. Supplementary data

Supplementary material related to this article can be found, in the online version, at <http://dx.doi.org/10.1016/j.apcatb.2014.04.013>.

References

- [1] A. Stanislaus, A. Marafi, M.S. Rana, *Catal. Today* 153 (2010) 1.
- [2] H. Topsøe, B.S. Clausen, F.E. Massoth, in: J.R. Anderson, M.V. Boudart (Eds.), *Hydrotreating Catalysis*, vol. 11, Springer-Verlag, Berlin-Heidelberg-N.Y., 1996, p. 310p.
- [3] H. Hallie, *Oil Gas J.* 48 (1982) 69.
- [4] R. Prada Silvy, P. Grange, F. Delannay, B. Delmon, *Appl. Catal.* 46 (1989) 113.
- [5] J. Van Gestel, J. Leglise, J.C. Duchet, *J. Catal.* 145 (1994) 429.
- [6] J.G. Welch, P. Poyner, R.F. Skelly, *Oil Gas J.* 92 (1994) 56.
- [7] F. Labruyere, P. Dufresne, M. Lacroix, M. Breyssse, *Catal. Today* 43 (1998) 111.
- [8] S. Yamada, W. Qian, A. Ishihara, G. Wang, L. Li, T. Kabe, *Sekiyu Gakkaishi* 44 (2001) 217.
- [9] C. Glasson, C. Geantet, M. Lacroix, F. Labruyere, P. Dufresne, *J. Catal.* 212 (2002) 76.
- [10] S. Texier, G. Berhault, G. Perot, F. Diehl, *Appl. Catal. A* 293 (2005) 105.
- [11] A. Spojakina, E. Kraleva, K. Jiratova, L. Petrov, *Appl. Catal. A* 288 (2005) 10.
- [12] E. Kraleva, A. Spojakina, K. Jiratova, L. Petrov, *Catal. Lett.* 112 (2006) 203.
- [13] A. Spojakina, K. Jiratova, N. Kostova, J. Kocianova, M. Stamenova, *Kinet. Catal.* 44 (6) (2003) 13.
- [14] R. Shafi, M.R.H. Siddiqui, G.J. Hutchings, E.G.I.V. Derouane, Kozhevnikov, *Appl. Catal. A* 204 (2000) 251.
- [15] B. Pawelec, R. Mariscal, J.L.G. Fierro, A. Greenwood, P.T. Vasudevan, *Appl. Catal. A* 206 (2001) 295.
- [16] P. Blanchard, C. Lamonier, A. Griboval, E. Payen, *Appl. Catal. A* 322 (2007) 33.
- [17] P.A. Nikul'shin, A.V. Mozhaev, D.I. Ishutenko, P.P. Minaev, A.I. Lyashenko, A.A. Pimerzin, *Kinet. Catal.* 53 (5) (2012) 620.
- [18] N.N. Tomina, P.A. Nikul'shin, A.A. Pimerzin, *Petrol. Chem.* 48 (2) (2008) 92.
- [19] N.N. Tomina, P.A. Nikul'shin, A.A. Pimerzin, *Kinet. Catal.* 49 (5) (2008) 653.
- [20] P.A. Nikul'shin, A.V. Mozhaev, A.A. Pimerzin, N.N. Tomina, V.V. Konovalov, V.M. Kogan, *Kinet. Catal.* 52 (6) (2011) 862.
- [21] A.V. Mozhaev, P.A. Nikul'shin, A.I.A. Pimerzin, V.V. Konovalov, A.A. Pimerzin, *Petrol. Chem.* 52 (1) (2012) 41.
- [22] N.N. Tomina, P.A. Nikul'shin, V.S. Tsvetkov, A.A. Pimerzin, *Kinet. Catal.* 50 (2) (2009) 220.
- [23] P.A. Nikul'shin, N.N. Tomina, A.A. Pimerzin, A.V. Kucherov, V.M. Kogan, *Catal. Today* 149 (2010) 82.
- [24] P.A. Nikul'shin, N.N. Tomina, A.A. Pimerzin, A.Yu. Stakheev, I.S. Mashkovsky, V.M. Kogan, *Appl. Catal. A* 393 (2011) 146.
- [25] P.A. Nikul'shin, V.A. Salnikov, A.V. Mozhaev, P.P. Minaev, V.M. Kogan, A.A. Pimerzin, *J. Catal.* 309 (2014) 386.
- [26] C.I. Cabello, F.M. Cabrerizo, A. Alvarez, H.J. Thomas, *J. Mol. Catal. A* 186 (2002) 89.
- [27] I.L. Botto, C.I. Cabello, H.J. Thomas, *Mater. Chem. Phys.* 47 (1997) 37.
- [28] C.I. Cabello, I.L. Botto, H.J. Thomas, *Appl. Catal. A* 197 (2000) 79.
- [29] I. Pettiti, I.L. Botto, C.I. Cabello, S. Colonna, M. Faticanti, G. Minelli, P. Porta, H.J. Thomas, *Appl. Catal. A* 220 (2001) 113.
- [30] J. Mazurelle, C. Lamonier, E. Payen, D. Guillaume, *Catal. Today* 130 (2008) 130, 41.
- [31] C. Lamonier, C. Martin, J. Mazurelle, V. Harlé, D. Guillaume, E. Payen, *Appl. Catal. B* 70 (2007) 548.
- [32] A. Griboval, P. Blanchard, E. Payen, M. Fournier, J.L. Dubois, *Catal. Today* 45 (1998) 277.
- [33] D. Soogund, Ph. Lecour, A. Daudin, B. Guichard, Ch. Legens, C. Lamonier, E. Payen, *Appl. Catal. B* 98 (2010) 39.
- [34] J.A.R. Van Veen, P.A.J.M. Hendriks, R.R. Andrea, E.J.G.M. Romers, A.E.J. Wilson, *Phys. Chem.* 94 (1990) 5275.
- [35] P.A. Nikul'shin, D.I. Ishutenko, A.V. Mozhaev, K.I. Maslakov, A.A. Pimerzin, *J. Catal.* 312 (2014) 152.
- [36] A.V. Mozhaev, P.A. Nikul'shin, V.V. Konovalov, Yu.V. Eremina, A.A. Pimerzin, 5th International Symposium on the Molecular Aspects of Catalysis by Sulfides (MACS-5), 30 May–3 June 2010, Copenhagen, Denmark.
- [37] P.A. Nikul'shin, A.V. Mozhaev, A.I.A. Pimerzin, V.V. Konovalov, A.A. Pimerzin, *Fuel* 100 (2012) 24.
- [38] V.M. Kogan, P.A. Nikul'shin, N.N. Rozhdestvenskaya, *Fuel* 100 (2012) 2.
- [39] V.M. Kogan, P.A. Nikul'shin, *Catal. Today* 149 (2010) 224.
- [40] M.T. Pope, *Heteropoly and Isopoly Metallates*, Springer, Berlin, 1983, pp. 232.
- [41] G. Brauer (Ed.), *Handbuch der präparativen anorganischen Chemie*, vol. 6, Mir, Moscow, 1986.
- [42] S. Kasztelan, H. Toulhoat, J. Grimbölt, J.P. Bonnelle, *Appl. Catal.* 13 (1984) 127.
- [43] E.J.M. Hensen, P.J. Kooyman, Y. van der Meer, A.M. van der Kraan, V.H.J. de Beer, J.A.R. van Veen, R.A. van Santen, *J. Catal.* 199 (2001) 224.
- [44] D. Ferdous, A.K. Dalai, J. Adjaye, L. Kotlyar, *Appl. Catal. A* 294 (2005) 80.
- [45] M. Li, H. Li, F. Jiang, Y. Chu, H. Nie, *Catal. Today* 149 (2010) 35.
- [46] A. Gandubert, C. Legens, D. Guillaume, S. Rebours, E. Payen, *Oil Gas Sci. Technol.-Rev. IFP* 62 (1) (2007) 79.
- [47] A.D. Gandubert, E. Krebs, C. Legens, D. Costa, D. Guillaume, P. Raybaud, *Catal. Today* 130 (2008) 149.
- [48] J. Ancheyta, G. Marroquin, M.J. Angeles, M.J. Macias, I. Pitault, M. Forissier, R.D. Morales, *Energy Fuels* 16 (2002) 1059.
- [49] N. Rinaldi, T. Kubota, Y. Okamoto, *Ind. Eng. Chem. Res.* 48 (2009) 10414.
- [50] J.C. Dupin, D. Gonbeau, I. Martin-Litas, Ph. Vinatier, A. Levasseur, *Appl. Surf. Sci.* 173 (2001) 140.
- [51] A.M. Venezia, *Catal. Today* 77 (2003) 359.
- [52] I. Alstrup, I. Chorkendorff, R. Candia, B.S. Clausen, H. Topsøe, *J. Catal.* 77 (1982) 397.
- [53] A.M. de Jong, V.H.J. (San) de Beer, J.A. Rob van Veen, J.W. (Hans) Niemantsverdriet, *J. Phys. Chem.* 100 (1996) 17722.
- [54] N. Frizi, P. Blanchard, E. Payen, P. Baranek, C. Lancelot, M. Rebeilleau, C. Dupuy, J.P. Dath, *Catal. Today* 130 (2008) 32.
- [55] P. Mazoyer, C. Geantet, F. Diehl, S. Lordinat, M. Lacroix, *Catal. Today* 130 (2008) 75.
- [56] L. Coulier, V.H.J. de Beer, J.A.R. van Veen, J.W. Niemantsverdriet, *J. Catal.* 197 (2001) 26.
- [57] M.A. Lélias, P.J. Kooyman, L. Mariey, L. Oliviero, A. Travert, J. van Gestel, J.A.R. van Veen, F. Maugé, *J. Catal.* 267 (2009) 14.
- [58] J. Escobar, M.C. Barrera, J.A. Toledo, M.A. Cortes-Jacome, C. Angeles-Chavez, S. Nunez, V. Santes, E. Gomez, L. Diaz, E. Romero, J.G. Pacheco, *Appl. Catal. B* 88 (2009) 564.
- [59] H. Li, M. Li, Y. Chu, F. Liu, H. Nie, *Appl. Catal. A* 403 (2011) 75.
- [60] D. Valencia, T. Klimova, *Appl. Catal. B* 129 (2013) 137.
- [61] A. Tuxen, H. Gøbel, B. Hinnemann, Z. Li, K.G. Knudsen, H. Topsøe, J.V. Lauritsen, F. Besenbacher, *J. Catal.* 281 (2011) 345.
- [62] V.M. Kogan, R.G. Gaziev, S.W. Lee, N.N. Rozhdestvenskaya, *Appl. Catal. A* 251 (2003) 187.